GAUSSIAN MSK (GMSK)

The main problem with MSK is that it has high out-of-band spectral components.

∴ GMSK was proposed by NTT in 1981.
Application: Mobile Communications.

Ref. K. Murota and K. Hirade, "GMSK Modulation for Digital Mobile Radio Telephony," IEEE Trans. Commun. vol. COM-29, pp. 1044–1050, July 1981.

Transmitter

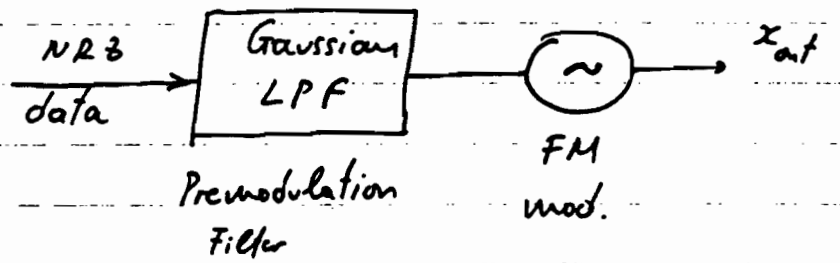

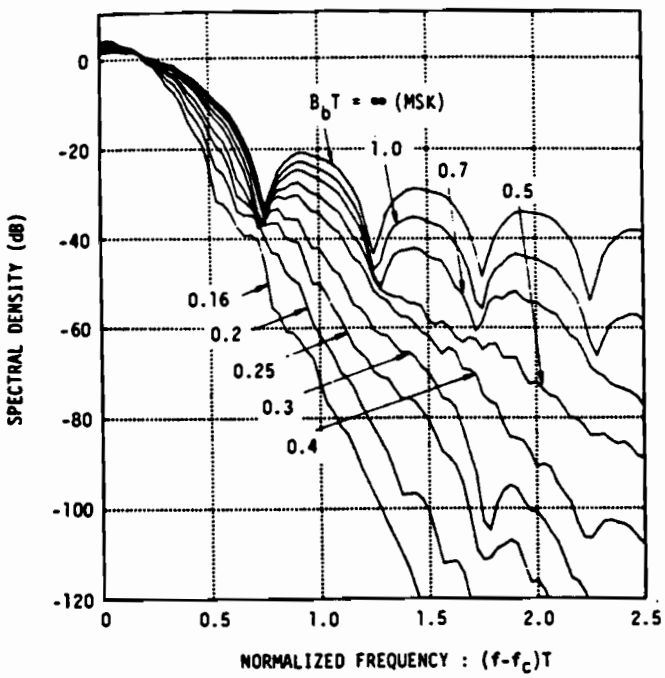

Fig. 2. Power spectra of GMSK.

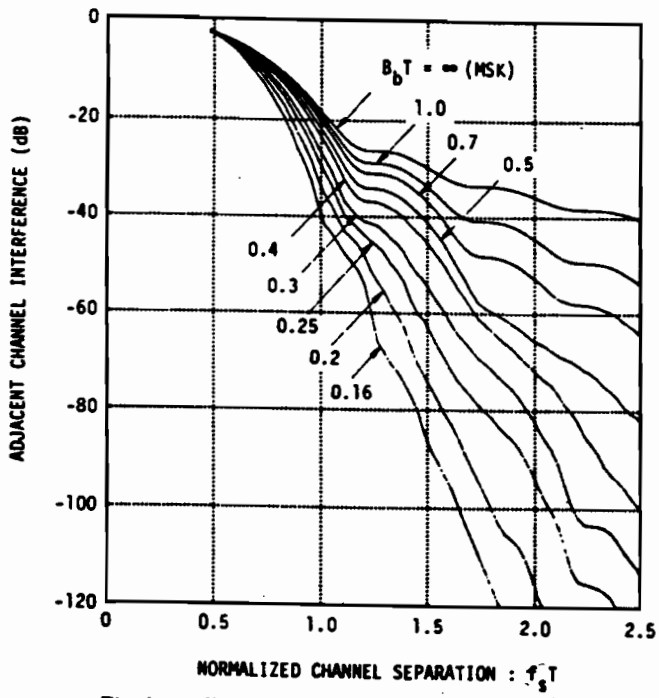

Fig. 4. Adjacent channel interference of GMSK.

TABLE I
OCCUPIED BANDWIDTH CONTAINING A GIVEN PERCENTAGE POWER

B_bT \ %	90	99	99.9	99.99
0.2	0.52	0.79	0.99	1.22
0.25	0.57	0.86	1.09	1.37
0.5	0.69	1.04	1.33	2.08
MSK	0.78	1.20	2.76	6.00
TFM	0.52	0.79	1.02	1.37

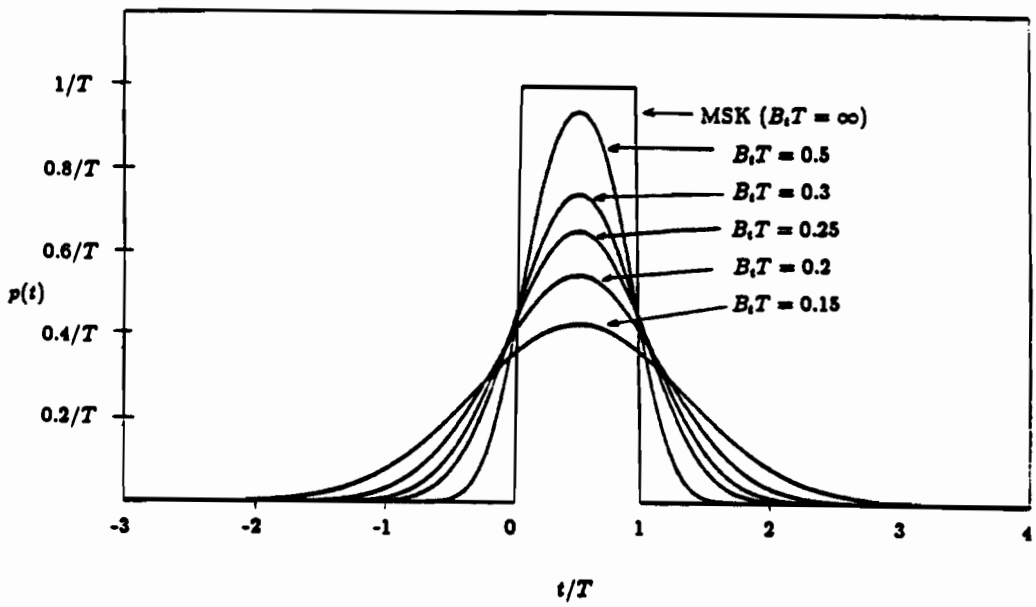

Figure 4.2: Pulse response of GLPF as a function of BT product.

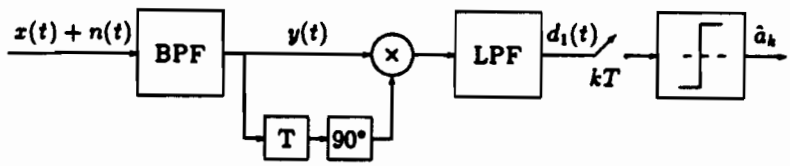

Fig. 2. Block diagram of a one-bit differential detector.

TABLE I

PHASE SHIFTS (IN DEGREES) CORRESPONDING TO SIGNAL θ_o AND ISI TERMS (θ_i, FOR $i \neq 0$) AS A FUNCTION OF TRANSMIT GAUSSIAN FILTER B_tT FOR THE ONE-BIT DIFFERENTIAL DETECTOR. $\Delta\theta_{min}$ AND $\Delta\theta_{min}^{DF}$ ARE THE MINIMUM DIFFERENTIAL PHASE ANGLES BEFORE AND AFTER APPLYING DECISION FEEDBACK

B_tT	θ_{-3}	θ_{-2}	θ_{-1}	θ_0	θ_1	θ_2	θ_3	$\Delta\theta_{min}$	$\Delta\theta_{min}^{DF}$
0.15	0.3	4.55	21.85	36.6	21.85	4.55	0.3	—	19.8
0.2	—	1.7	20.6	45.4	20.6	1.7	—	1.6	46.2
0.25	—	0.6	18.2	52.4	18.2	0.6	—	29.6	67.2
0.3	—	0.2	15.9	57.8	15.9	0.2	—	51.2	83.4
0.4	—	—	12.5	65.0	12.5	—	—	80.0	105.0
0.5	—	—	10.3	69.4	10.3	—	—	97.6	118.2
1.0	—	—	5.9	78.2	5.9	—	—	132.8	144.6
∞ (MSK)	—	—	—	90.0	—	—	—	180.0	180.0

GMSK → binary scheme ⇒ for high SNR

$$P_e = \frac{1}{2}\,\mathrm{erfc}\left(\frac{d_{min}}{2\sqrt{N_0}}\right)$$

$$d_{min} \rightarrow d^2 = \frac{1}{2}\int_{t_1}^{t_2} |u_m(t) - u_s(t)|^2\,dt$$

$u_m(t) \rightarrow 1$

$u_s(t) \rightarrow -1$

$$E = \frac{1}{2}\int_0^T |u_m(t)|^2 dt = \frac{1}{2}\int_0^T |u_s(t)|^2 dt$$

For $B_b T \rightarrow \infty$ ⇒ MSK ⇒ $d_{min} = 2\sqrt{E_b}$

Otherwise the observation interval $t_2 - t_1$ will be longer than 2

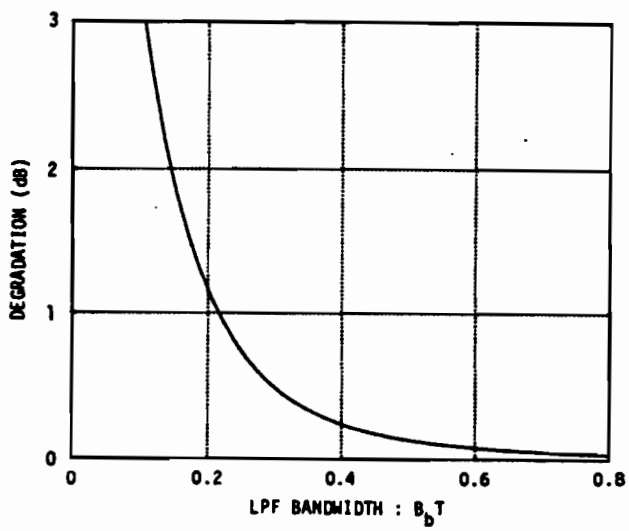

Fig. 6. Theoretical E_b/N_0 degradation of GMSK.

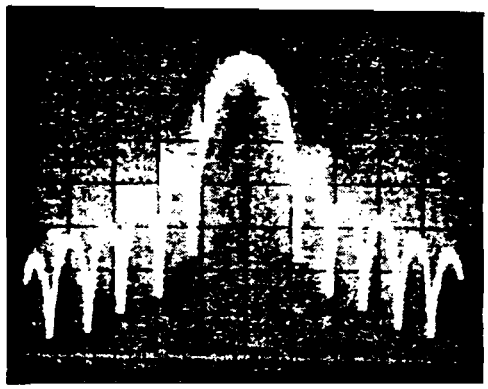

$B_bT = \infty$ (MSK)

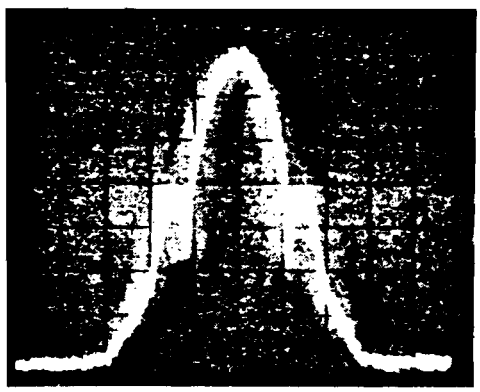

$B_bT = 0.5$

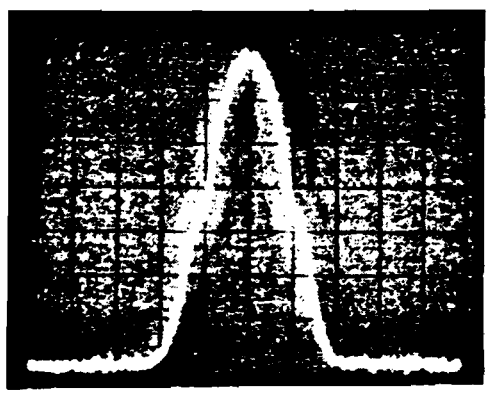

$B_bT = 0.25$

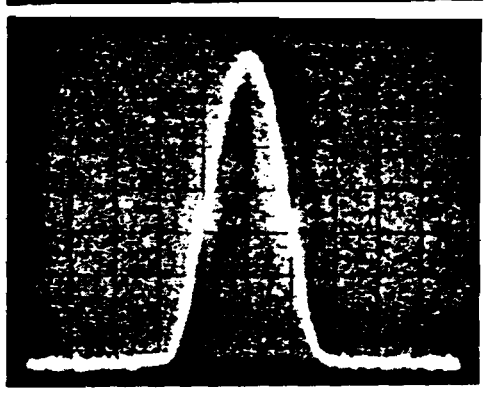

$B_bT = 0.2$

Fig. 10. Measured power spectra of GMSK (*V*: 10 dB/div., *H*: 10 kHz/div.).

Rx → Carrier & Symbol

One approach would be a system similar to MSK
Another - " - - - employing differential detection.

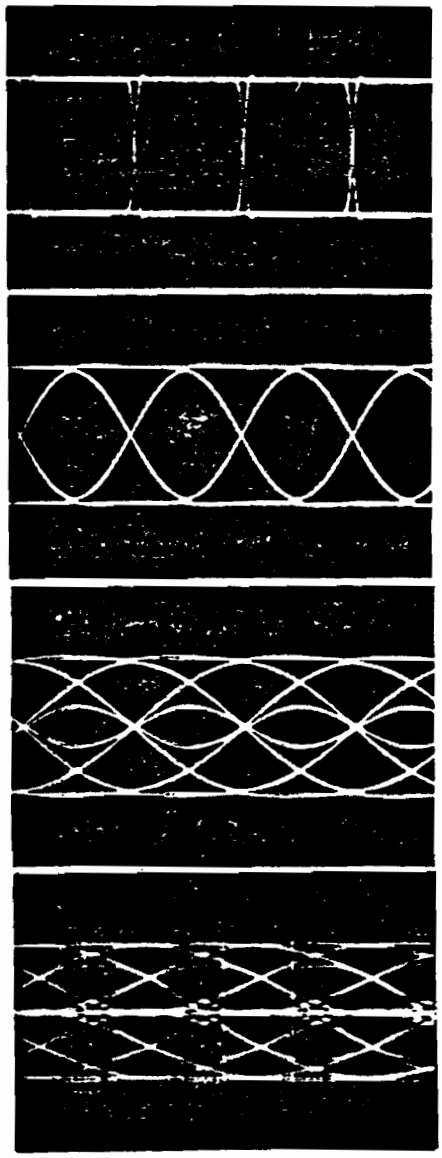

Fig. 11. Instantaneous frequency variation of GMSK.

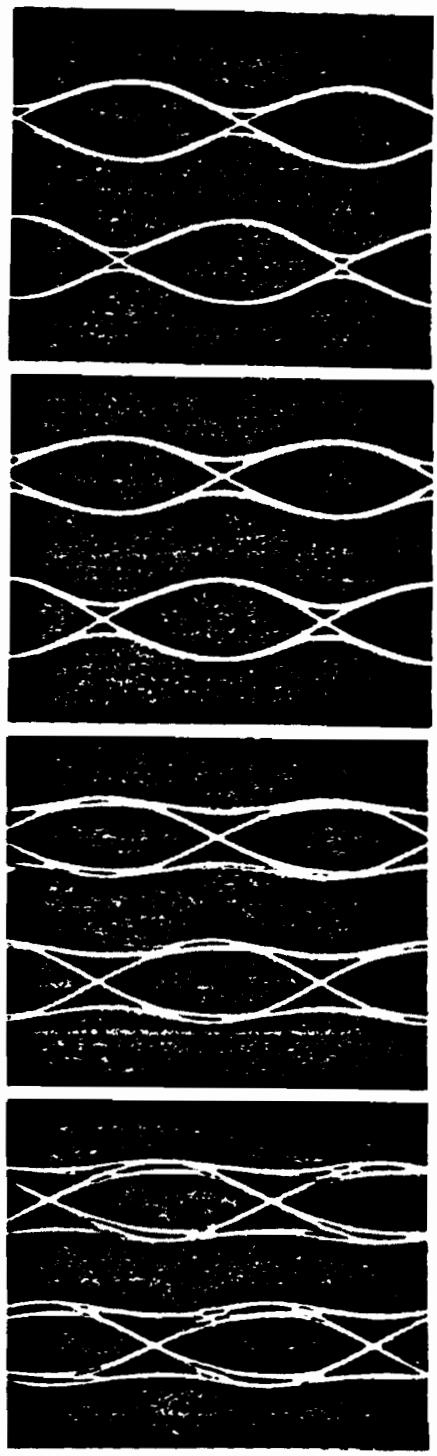

Fig. 12. GMSK eye patterns demodulated by orthogonal coherent detector.

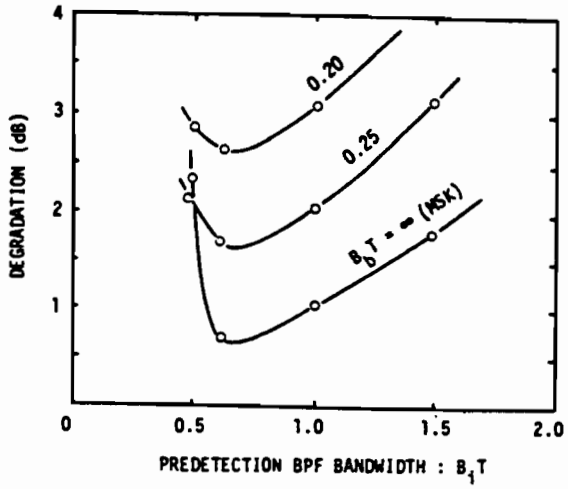

Fig. 14. Degradation of required E_b/N_0 for obtaining BER of 10^{-3}.

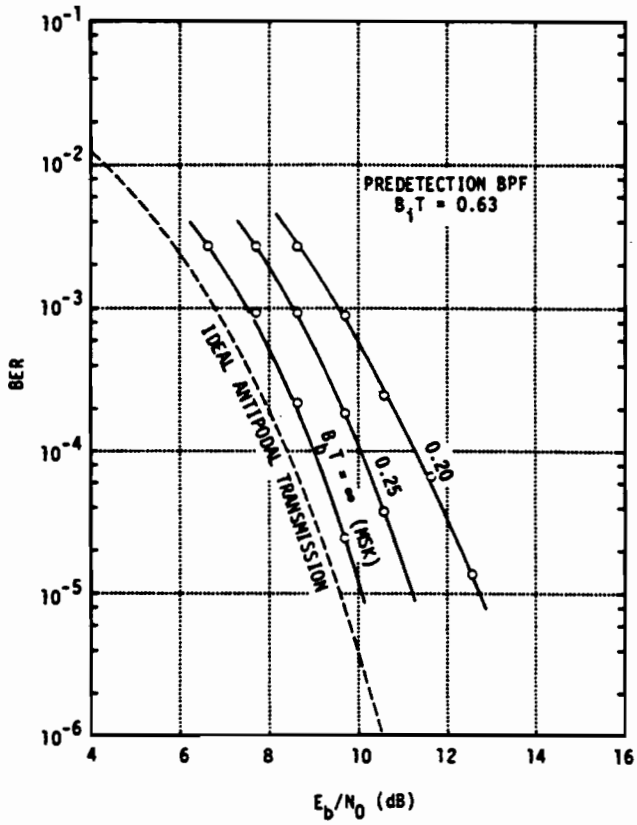

Fig. 13. Static BER performance.

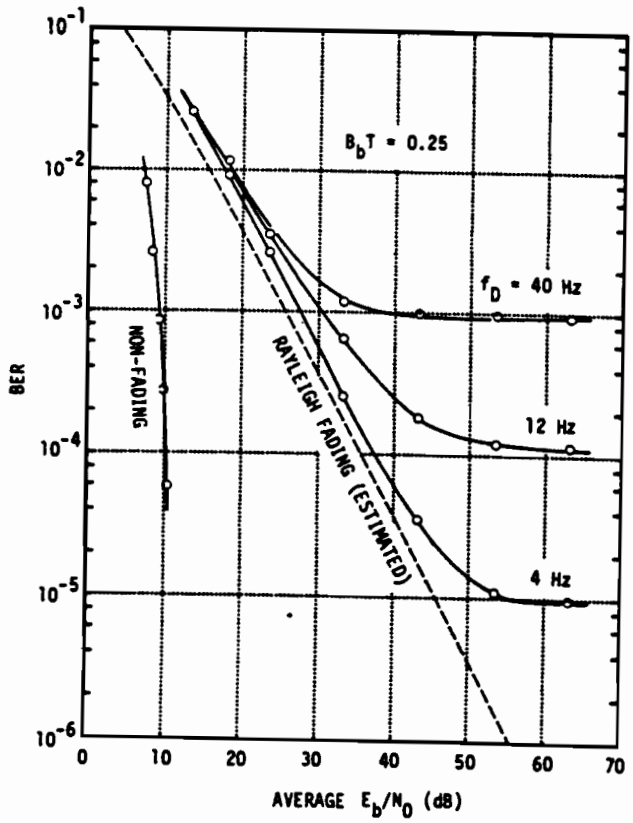

Fig. 15. Dynamic BER performance.

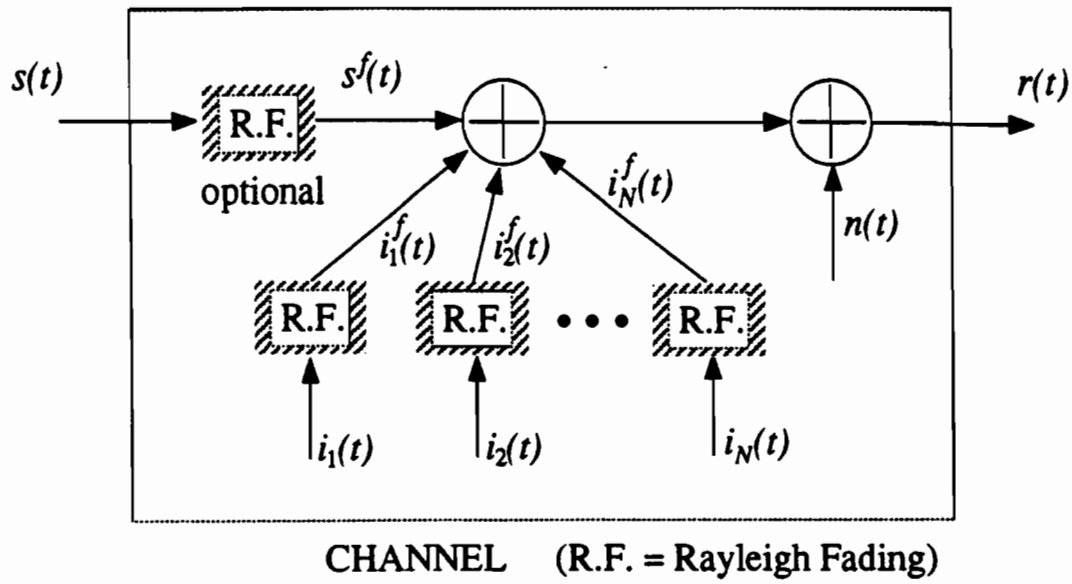

Figure 1 Block diagram of the channel model.

Ref. S. S. Shin and P. T. Mathiopoulos
"Differentially detected GMSK signals in CCI channels for mobile cellular telecommunication systems"
August 1993 issue of the IEEE Transactions on Vehicular Technology.

(also pp. 76B - 76F)

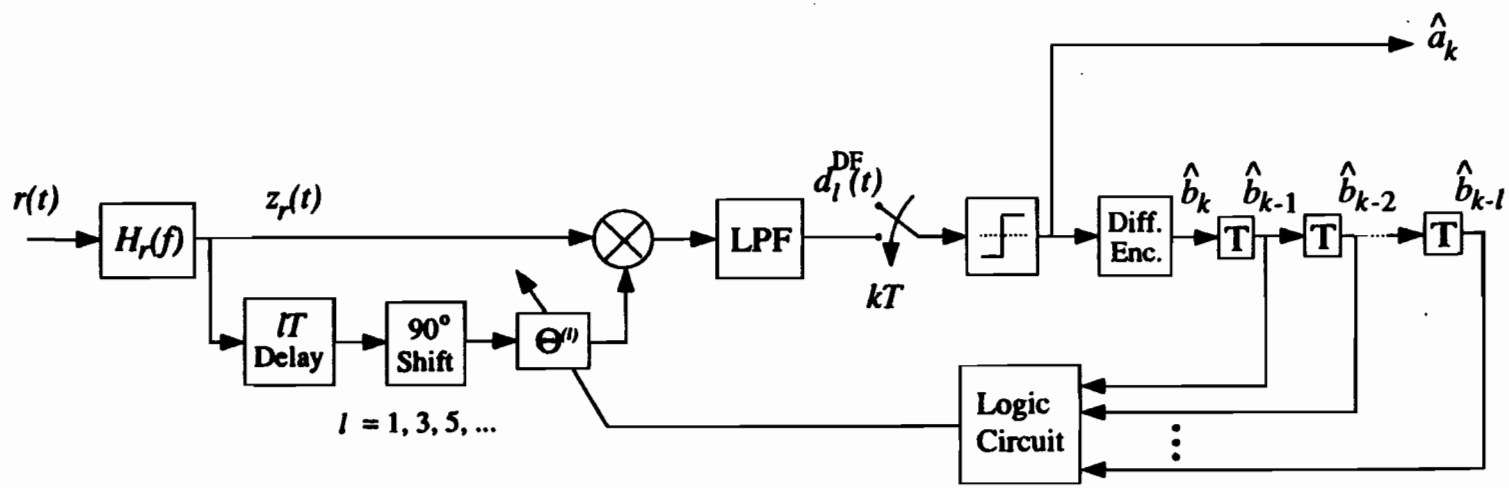

Figure 2 Block diagram of the l-bit differential detection receiver employing the decision feedback (DF) technique.

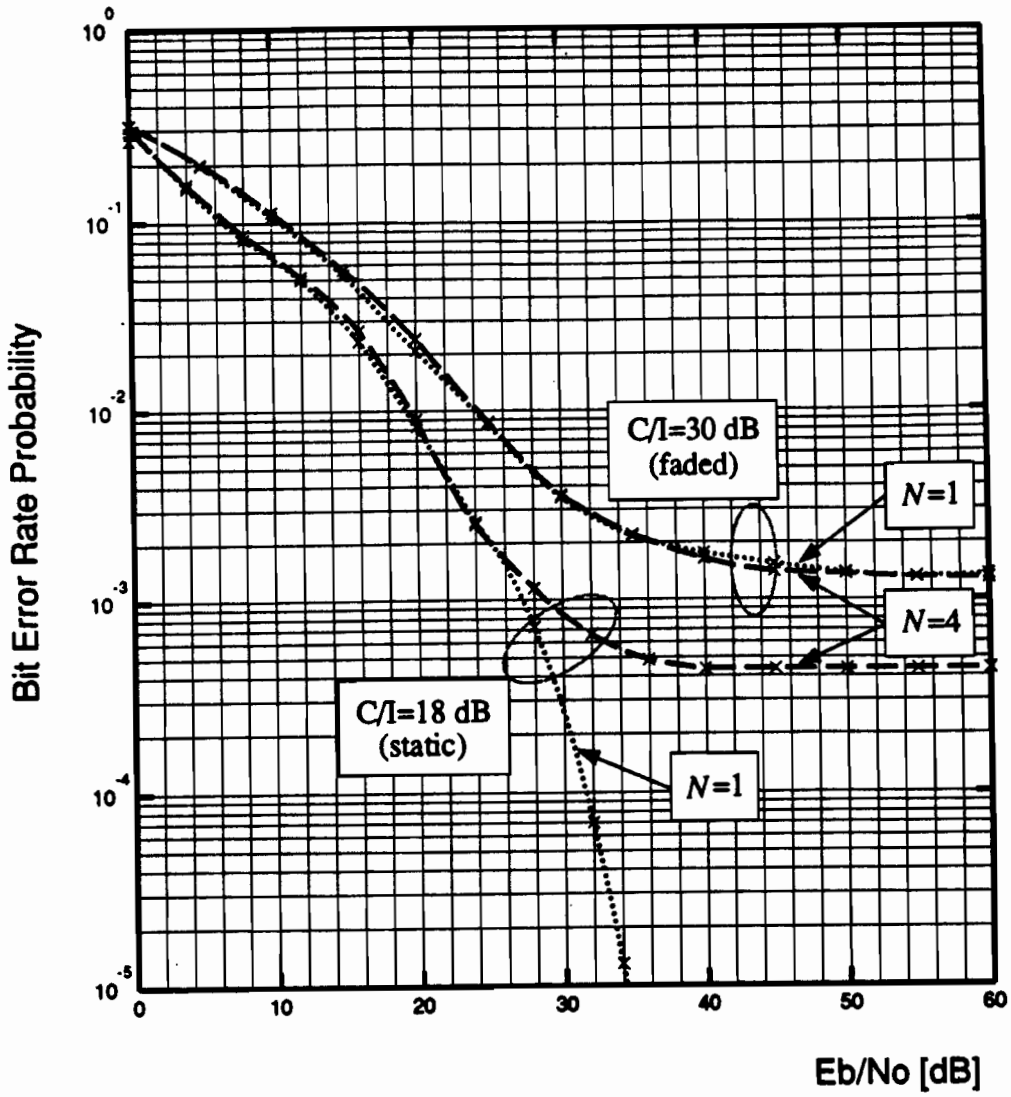

Figure 3 BER performance of conventional 1-bit differentially detected GMSK scheme operated in the presence of static and Rayleigh faded CCI with $N = 1$ and $N = 4$.

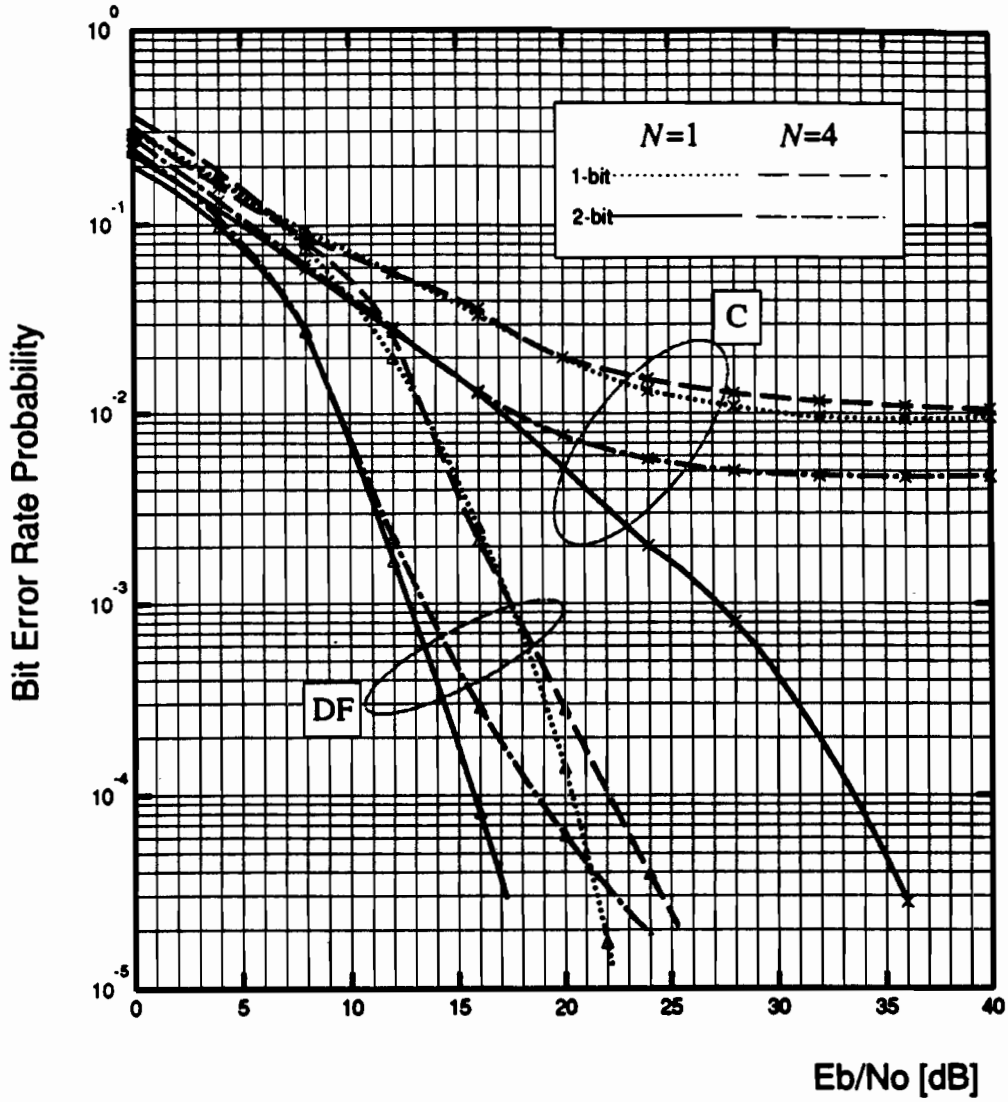

Figure 4 BER performance of the conventional (C) and decision feedback (DF) 1- and 2-bit differential detection receiver in the presence of static CCI (C/I = 14 dB) with $N = 1$ and $N = 4$.

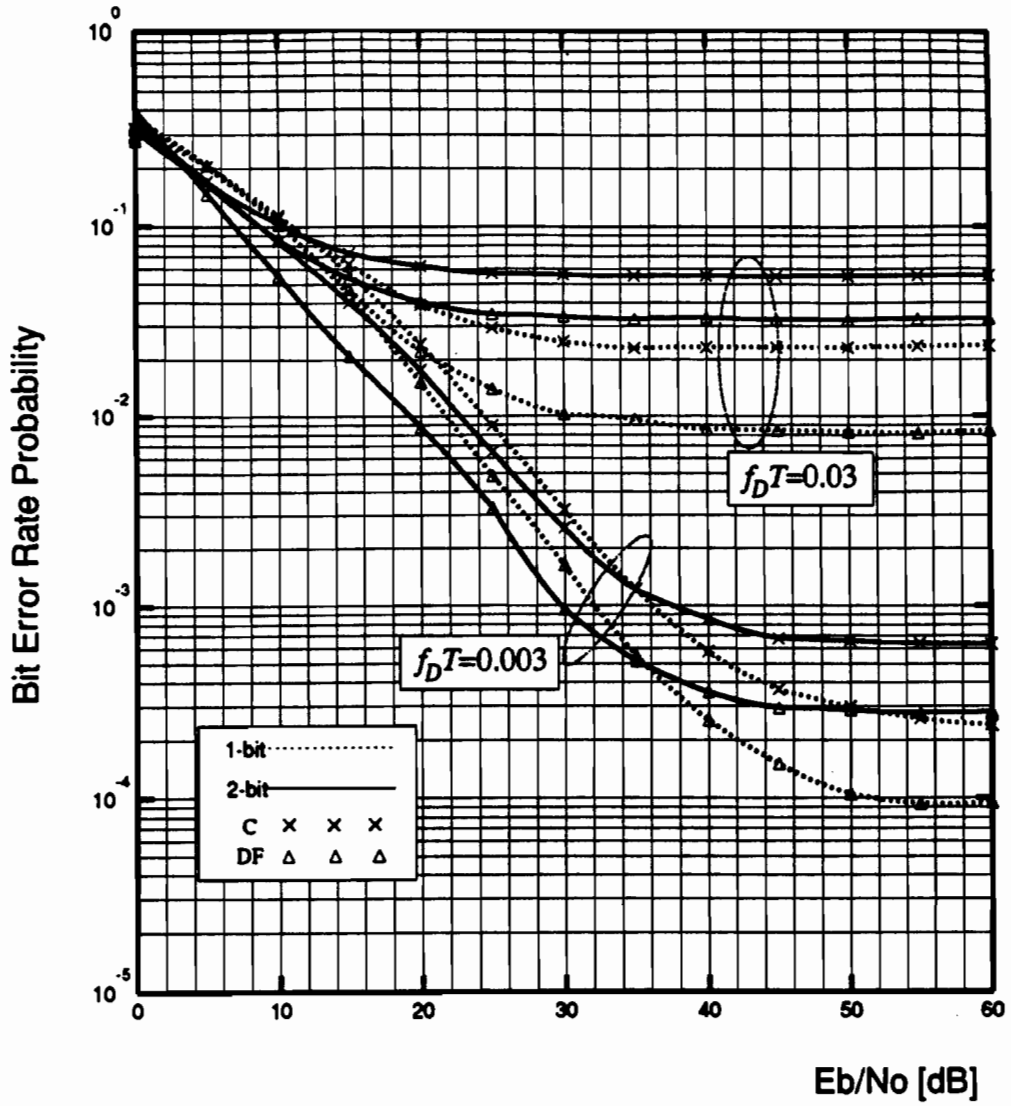

Figure 5 BER performance of the conventional (C) and decision-feedback (DF) 1- and 2-bit differential detection receivers in the presence of fading ($C/I \rightarrow \infty$).

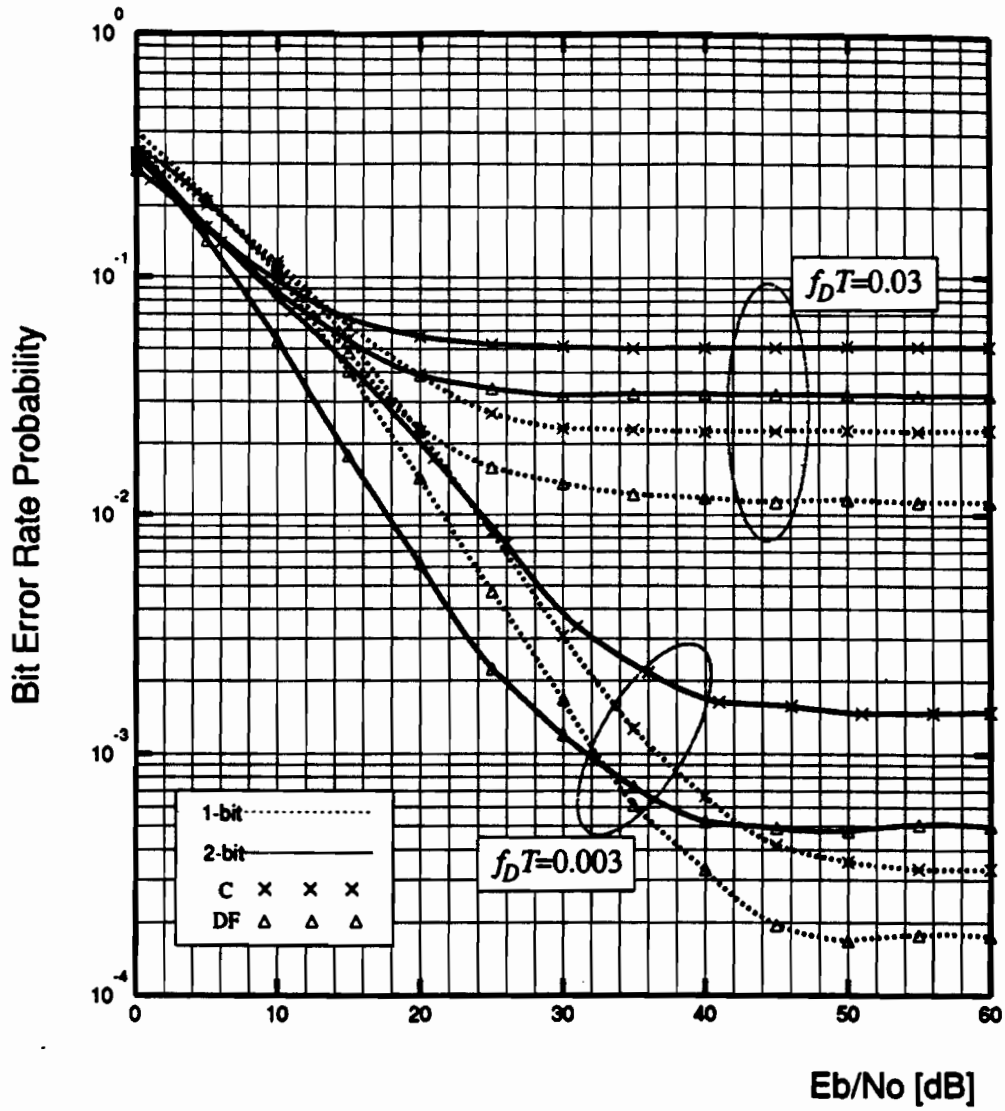

Figure 6 BER performance of the conventional (C) and decision-feedback (DF) 1- and 2-bit differential detection receivers in the presence of faded CCI (C/I = 40 dB).

CONTINUOUS PHASE MODULATION (CPM)

Ref. C-E Sundberg, "Continuous Phase Modulation," IEEE Communication Magazine, vol. 24, pp. 25-38, April 1986.

- Improve MSK while maintaining constant amplitude.
  - : narrower spectrum, lower spectral sidelobes, better BER (or combination of all).

$$s(t) = \sqrt{\frac{2E}{T}} \cos\left[2\pi f_c t + \underbrace{\phi(t, \underline{\alpha})}_{\text{info}}\right]$$

E : energy/symbol ; T: symbol duration ; f_c : carrier frequency.

$$\phi(t, \underline{\alpha}) = 2\pi h \sum_{i=-\infty}^{\infty} \alpha_i \, q(t - iT) \; ; \; q(t) = \int_{-\infty}^{t} g(\tau) d\tau$$

- h : modulation index
- $g(t)$: a smooth pulse shape over a finite interval $0 \le t \le LT$
- $\alpha_i \in \{\pm 1, \pm 3, \ldots, \pm (M-1)\}$ – data symbols
- Normalization $\int_{-\infty}^{\infty} g(t) dt = \frac{1}{2}$ $\Rightarrow$ max phase shift over any symbol interval is $(M-1)h\pi$

°° By choosing $g(t)$ & varying h, M $\Rightarrow$ many, many CPM signals

TABLE I
Definition of the frequency pulse functions $g(t)$ used in this paper. By varying a, b and $g_0(t)$, the class of GTFM pulses is obtained.

LRC	$g(t) = \begin{cases} \frac{1}{2LT}\left[1 - \cos\frac{2\pi t}{LT}\right) & ; 0 \le t \le LT \\ 0 & ; \text{otherwise} \end{cases}$ L is the pulse length, e.g., 3RC has $L=3$.
TFM	$g(t) = \frac{1}{8}\left[a g_0(t-T) + b g_0(t) + a g_0(t+T)\right]$ $; a = 1; b = 2$ $g_0(t) \sim \sin\left(\frac{\pi t}{T}\right)\left[\frac{1}{\pi t} - \frac{2 - \frac{2\pi t}{T}\cot\left(\frac{\pi t}{T}\right) - \frac{\pi^2 t^2}{T^2}}{\frac{24\,\pi t^3}{T^2}}\right]$
LSRC	$g(t) = \frac{1}{LT} \cdot \frac{\sin\left(\frac{2\pi t}{LT}\right)}{\frac{2\pi t}{LT}} \cdot \frac{\cos\left(\beta \cdot \frac{2\pi t}{LT}\right)}{1 - \left(\frac{4\beta}{LT} \cdot t\right)^2}$; $0 \le \beta \le 1$

GMSK	$g(t) = \frac{1}{2T}\left[Q\left(2\pi B_b \frac{t - \frac{T}{2}}{\sqrt{\ell n 2}}\right) - Q\left(2\pi B_b \frac{t + \frac{T}{2}}{\sqrt{\ell n 2}}\right)\right]$ $; 0 \le B_b T < \infty$ $Q(t) = \int_t^\infty \frac{1}{\sqrt{2\pi}} e^{-\tau^2/2}\, d\tau$
LREC	$g(t) = \begin{cases} \frac{1}{2LT} & ; 0 \le t \le LT \\ 0 & ; \text{otherwise} \end{cases}$ $L = 1$ yields 1REC which is most often referred to as CPFSK.

Comments

- MSK ≡ LREC with $L=1$, $M=2$, $h = \frac{1}{2}$
- Memory : i) choose a pulse with $L>1$ (partial response CPM)
  ii) If $L=1$, memory through phase continuity (full response CPM)
- At $nT \le t \le (n+1)T$

$$\phi(t, \underline{\alpha}) = 2\pi h \sum_{i=n-L+1}^{n} \alpha_i\, q(t - iT) + \theta_n = \theta(t, \underline{\alpha}) + \theta_n$$

$$\theta_n = h\pi \sum_{i=-\infty}^{n-L} \alpha_i \Big|_{\text{mod } 2\pi}$$

Examples

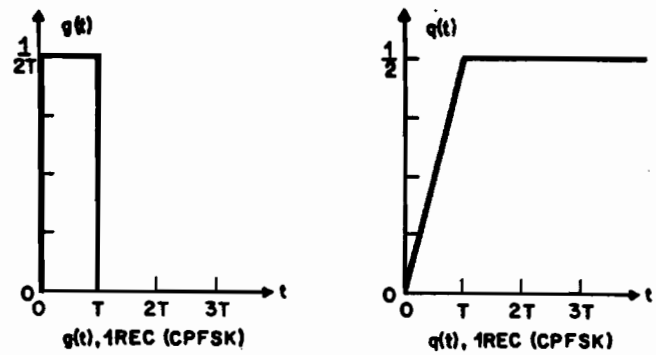

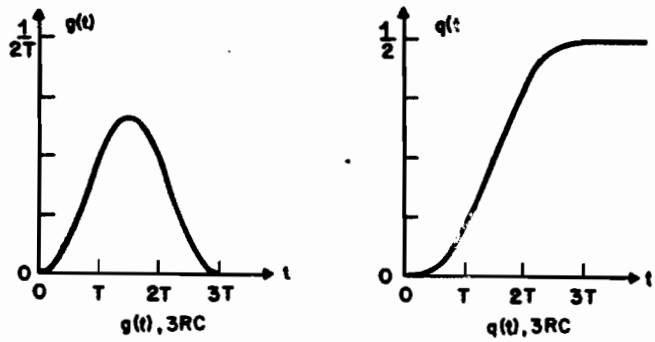

Fig. 1a. Pulse shapes g(t) (instantaneous frequency) and phase responses q(t) for the full response 1REC (CPFSK) and partial response 3RC CPM schemes.

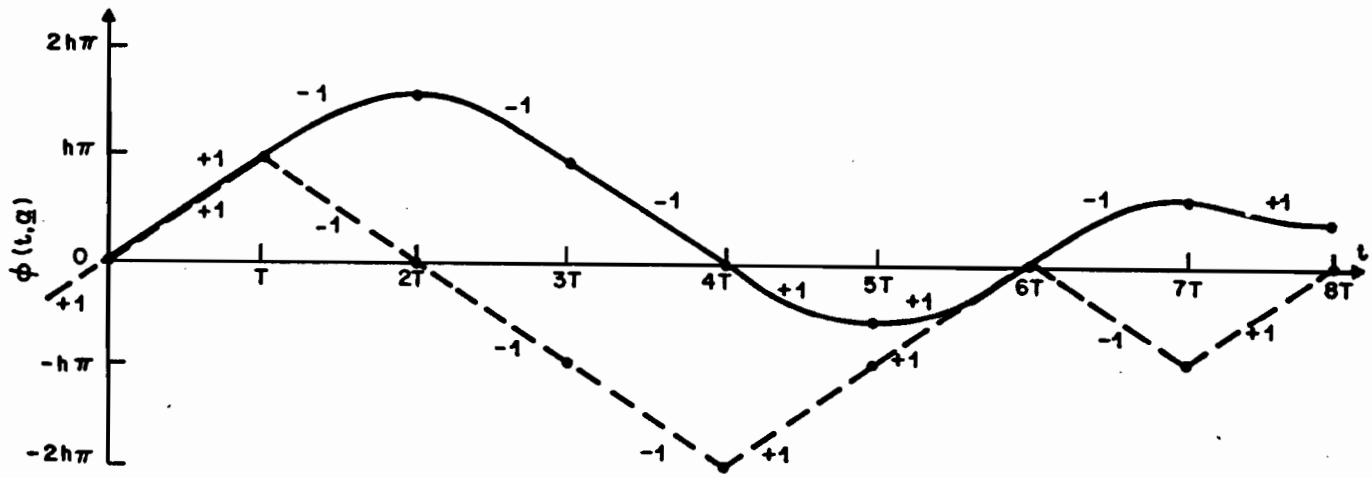

Fig. 1b. Examples of the information carrying phase function $\phi(t,\underline{\alpha})$ for 1REC (dashed) and 3RC (solid) for the data sequence +1, −1, −1, −1, +1, +1, −1, +1.

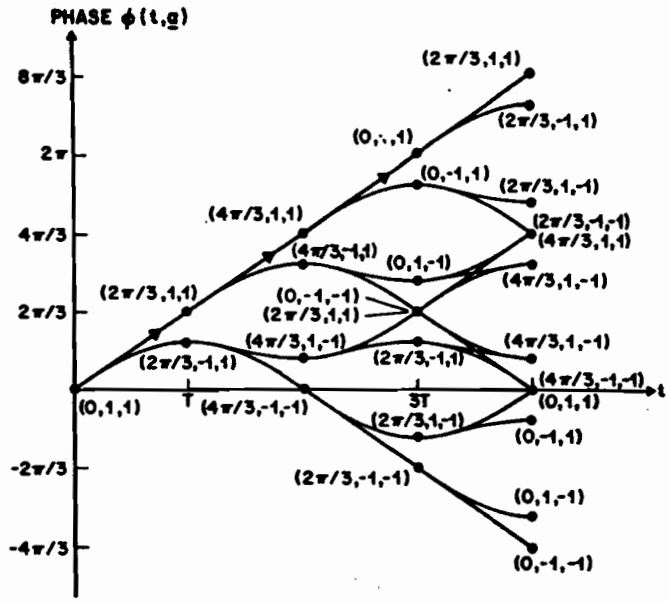

Fig. 1c. Phase tree for binary 3RC with h = 2/3. *The state description of the signal is also given. Notice the transitions with arrows. These are also shown in Figure 2a.*

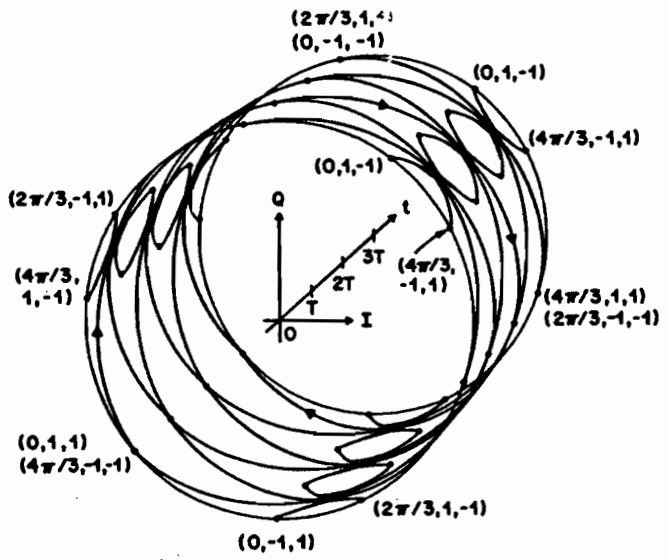

Fig. 2a. Phase-cylinder for M = 2, *3RC with* h = 2/3. *Compare the phase tree in Figure 1c. Note the arbitrary phase-offset between the phase in the tree in Figure 1c and the cylinder in Figure 2a. Also note that the tree is plotted over 4T and the cylinder over 3T. Notice the transitions with arrows. These are also shown in the tree in Figure 1c.*

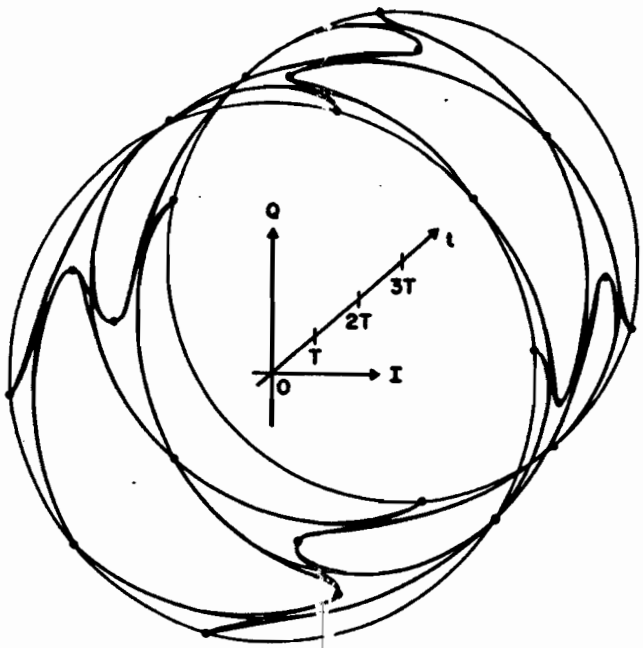

Fig. 2b. Phase cylinder for $M = 2$, *3RC*, $h = 1/2$.

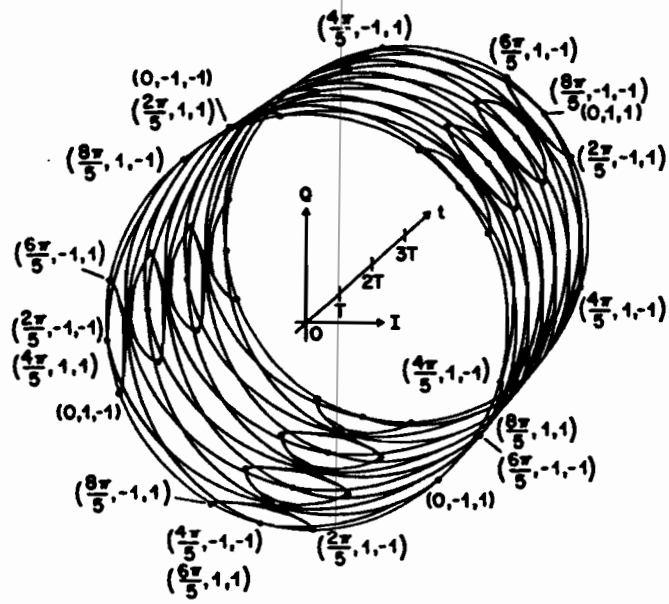

Fig. 2c. Phase cylinder for $M = 2$, *3RC with* $h = 4/5$.

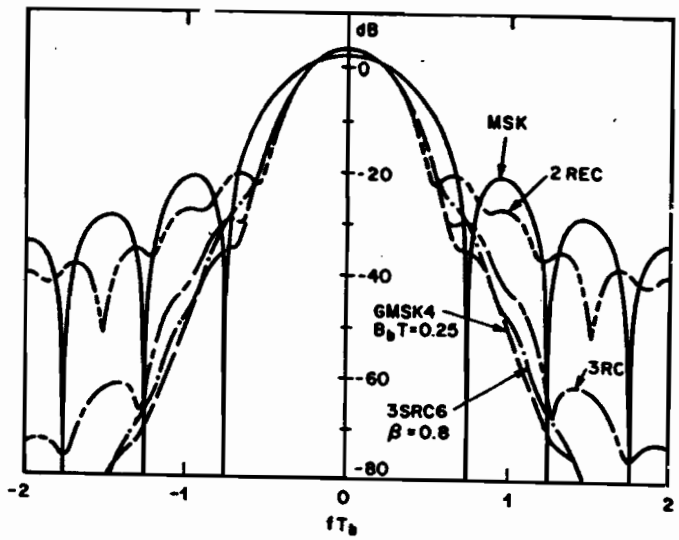

Fig. 3. Average power spectrum for some binary CPM schemes with h = 1/2, see Table 1.

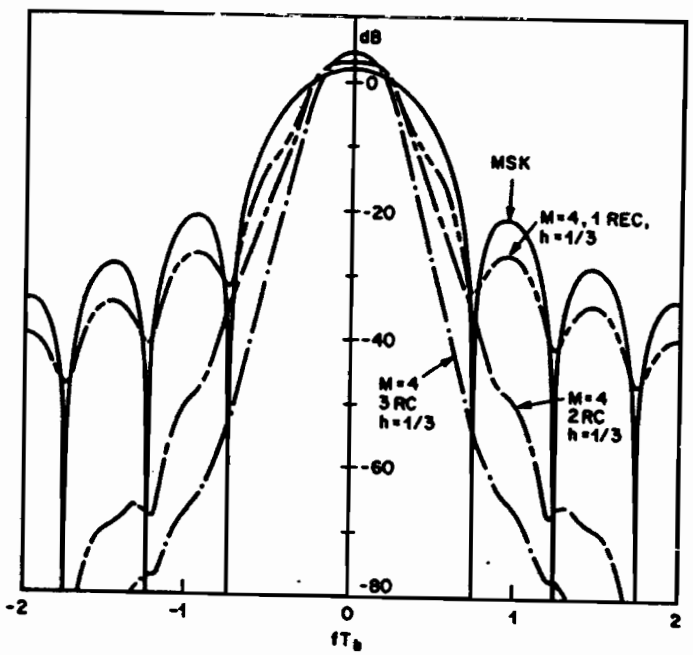

Fig. 4. Average power spectra for MSK (M=2, 1REC, h=1/2) and the M = 4, h = 1/3 schemes with 1REC, 2RC and 3RC pulses.

Width of main lobe ↓ with L ↑

↑ - { h ↑ / M ↑

Performance Evaluation

- Very difficult task in the general case

- For high SNR → find the minimum Euclidean distance between all possible pairs of signals

$$D_{min}^2 = d_{min}^2 \, 2E_b$$

$$= \min\left\{ 2E_b \log_2(M) \frac{1}{T} \int_0^{NT} [1 - \cos[\phi(t,\underline{\alpha}) - \phi(t,\underline{\beta})]] \, dt \right\}$$

NT receiver observation interval.

$$P_b \simeq C \, e^{-d_{min}^2 \frac{E_b}{N_0}} \qquad \text{(AWGN, coherent)}$$

C: const.

- Low SNR ⇒ computer simulation

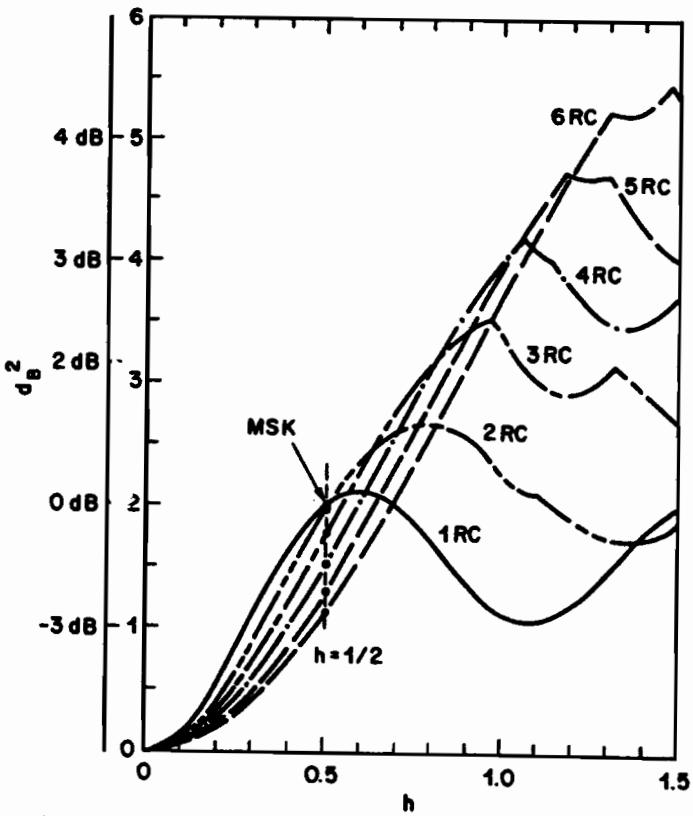

Fig. 5. Upper bound d_B^2 on the distance for the binary CPM schemes 1RC, 2RC, ···, 6RC.

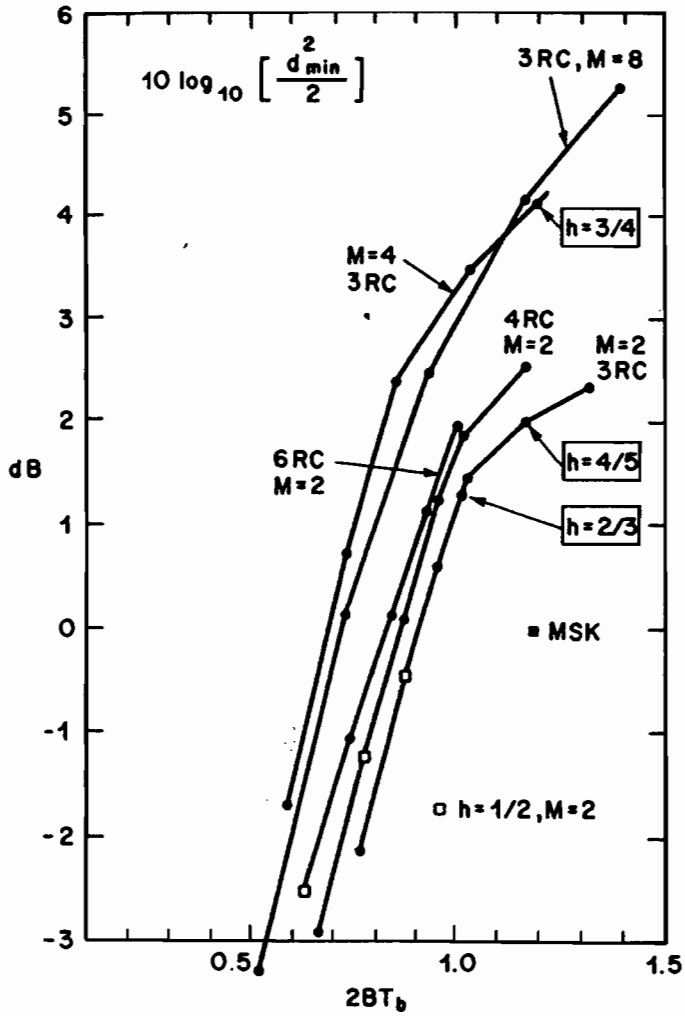

Fig. 6. Power-bandwidth tradeoff for CPM schemes using RC-pulses. The bandwidth is the 99% power in band definition. Note that the specific schemes are plotted as points and these are interconnected with straight lines.

Tx - Implementation

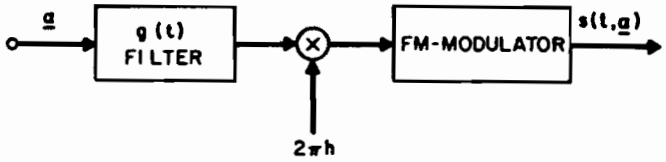

Fig. 7. Conceptual modulator for CPM directly based on Equation (1).

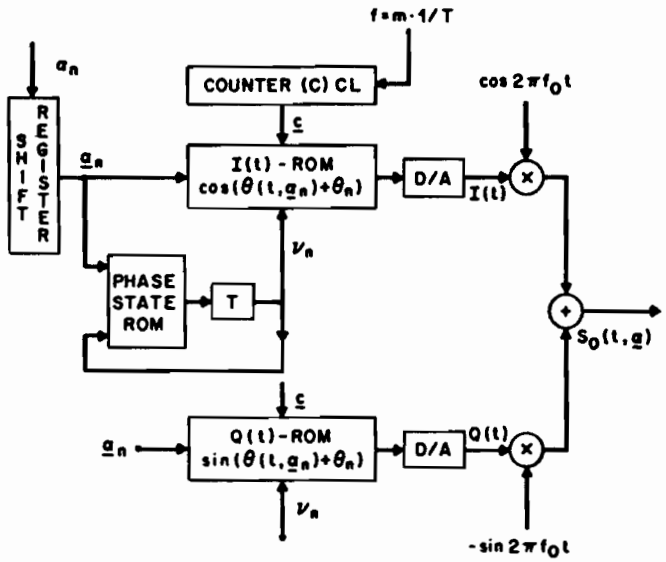

Fig. 8. General CPM transmitter based on the look-up table principle.

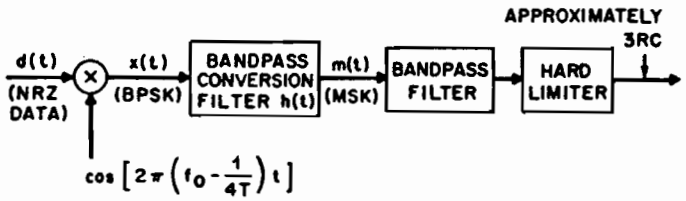

Fig. 9. Implementation of a serial MSK modulator utilizing a bandpass conversion filter. By proper bandpass filtering and hardlimiting an appropriate constant amplitude 3RC signal can be generated.

Rx - Implementation

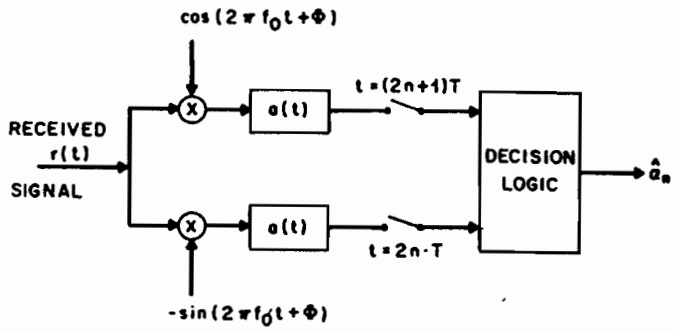

Fig. 12. Receiver structure for a parallel MSK-type receiver for h=1/2 CPM.

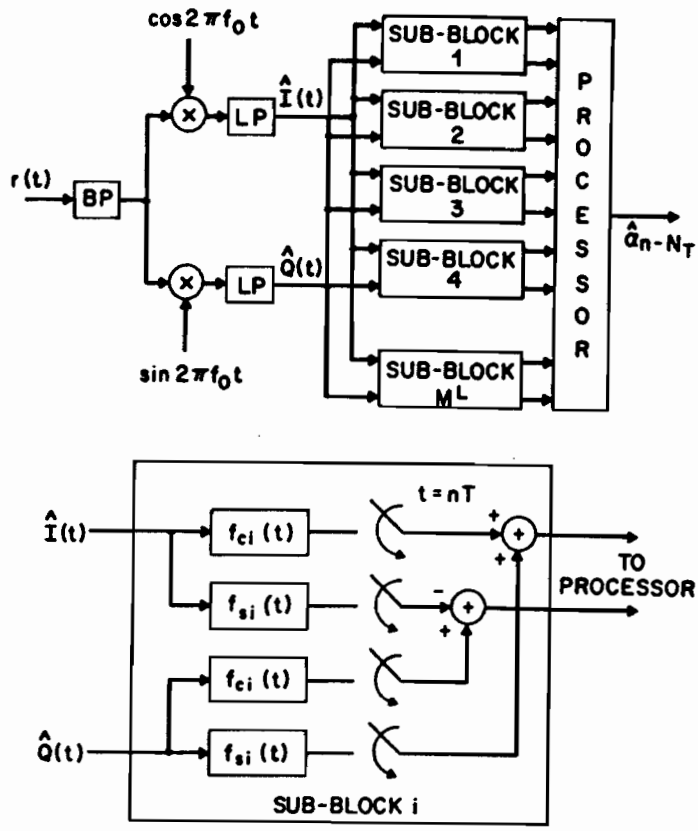

Fig. 10. A general Viterbi receiver structure for CPM. There are $4M^L$ linear filters.

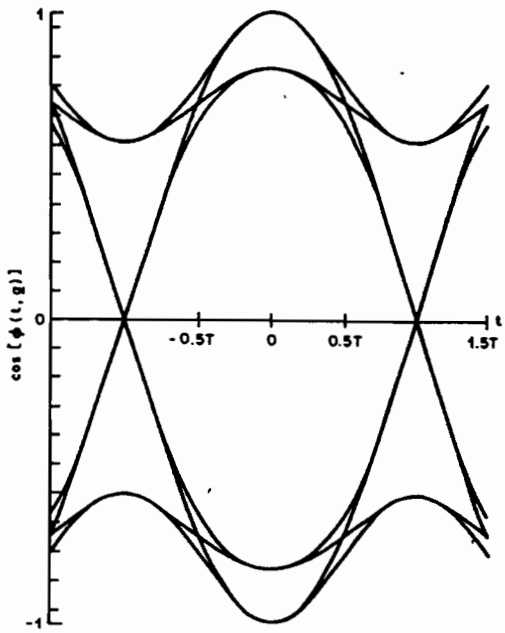

Fig. 13. Eye pattern for parallel MSK-type receiver for 3RC, h = 1/2.

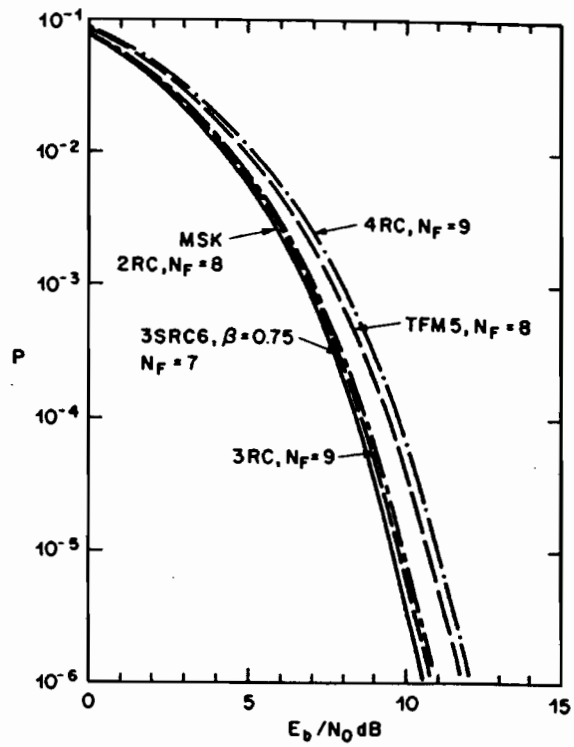

Fig. 15. The error probability for some binary, h = 1/2 CPM schemes. The MSK-type receivers use asymptotically optimum receiver filters for length N_f.

RELATIONS BETWEEN $\left[\frac{E_s}{N_0}\ ;\ \frac{E_b}{N_0}\right]$ & $\left[\frac{S}{N}\ ;\ \frac{C}{N}\right]$

E_b = Energy per bit [Joules]
E_s = " " symbol ["]
N_0 = Noise power spectral density (psd) $\left[\frac{\text{Watts}}{\text{Hz}}\right]$

S = Signal power (average) ← baseband [Watts]
C = Carrier " (") ← RF (modulated) ["]
N = Noise power (") ← over a certain bandwidth [Watts]

$$\left.\begin{array}{l} M \text{ symbols} \\ k \text{ bits/symbol} \end{array}\right) \Rightarrow M = 2^k$$

$$\left.\begin{array}{l} \text{Bit rate } f_b = \frac{1}{T_b} \\ \text{Symbol rate } f_s = \frac{1}{T_s} \end{array}\right) \Rightarrow T_s = k\,T_b \Rightarrow E_s = k\,E_b$$

Notes

① It is equivalent of having single-sided noise psd N_0 and double-sided noise psd, i.e., $N = N_0 \times (BW) = \frac{N_0}{2} \times 2(BW)$

② Since N is power ⇒ a bandwidth has to be specified. Usually this is the Nyquist bandwidth. However in practice this might be wider.

③ RF bandwidth is twice the equivalent baseband bandwidth

④ N_0 can be interpreted as the "1 Hz bandwidth noise power".

$$\frac{E_b}{N_0} = \frac{S\,T_b}{\frac{N}{BW}} = \left(\frac{S}{N}\right) T_b\,(BW) \equiv \left(\frac{C}{N}\right) T_b\,(BW)_{RF}$$

$$\frac{E_s}{N_0} = \frac{S\,T_s}{\frac{N}{BW}} = \left(\frac{S}{N}\right) T_s\,(BW) \equiv \underbrace{\left(\frac{C}{N}\right) T_s\,(BW)_{RF}}_{\text{Adds 3dB to the } \left(\frac{S}{N}\right)}$$

$\left(\frac{S}{N}\right) \triangleq$ signal-to-noise ratio ; $\left(\frac{C}{N}\right) \triangleq$ carrier-to-noise ratio

(BW) is in most cases the Nyquist bandwidth.

Example

f_b, Nyquist filters, $\frac{N_0}{2}$ double-sided psd. If $\frac{E_b}{N_0} = 8.4\,dB$ find the equivalent $\left(\frac{S}{N}\right)$ & $\left(\frac{C}{N}\right)$ for i) BPSK and ii) 16-QAM.

Solution

$$\frac{E_b}{N_0} = \left(\frac{S}{N}\right) T_b\,(BW) = \left(\frac{S}{N}\right) T_b\,\frac{1}{2T_s}$$

i) $T_s = T_b \Rightarrow \frac{E_b}{N_0} = \left(\frac{S}{N}\right)\frac{1}{2} \Rightarrow \left(\frac{S}{N}\right) = 11.4\,dB \Rightarrow \left(\frac{C}{N}\right) = 14.4\,dB$

ii) $T_s = 4T_b \Rightarrow \frac{E_b}{N_0} = \left(\frac{S}{N}\right)\frac{1}{8} \Rightarrow \left(\frac{S}{N}\right) = 17.4\,dB \Rightarrow \left(\frac{C}{N}\right) = 20.4\,dB$

M-ary PAM - (Performance)

- a_k : equiprobable symbols taking values from the alphabet

$$\underbrace{\pm d, \pm 3d, \ldots, \pm (M-1)d}_{M\text{-values}} \quad (M = 2^k)$$

- Rate: $\frac{1}{T_s} = \frac{1}{T}$ and $T = k\,T_b$

- AWGN, $\frac{N_0}{2}$ - double sided

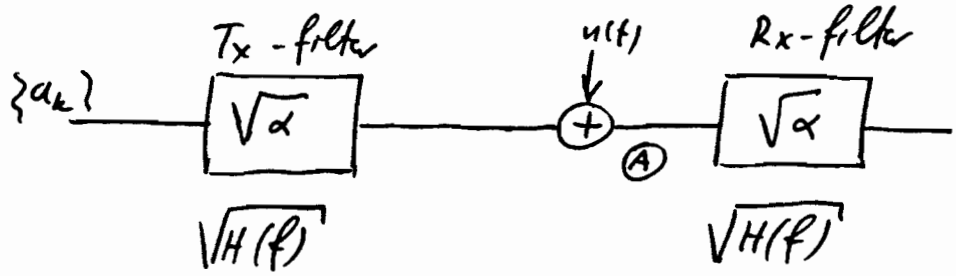

(Note:

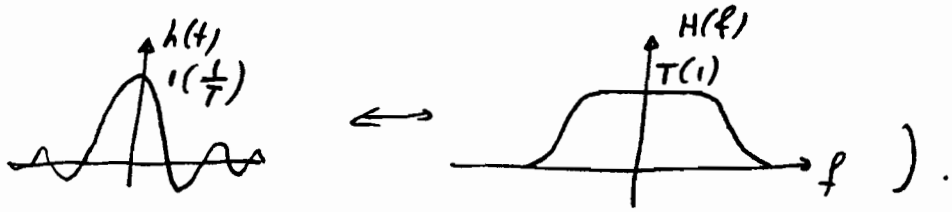

).

Power at (A) $\quad P_s = \frac{\overline{a^2}}{T} \int_{-\infty}^{\infty} H(f)\,df = \frac{\overline{a^2}}{T}$

$$\overline{a^2} = \frac{2\times d^2 + 2\times(3d)^2 + \ldots + 2\times(M-1)^2 d^2}{M} = \frac{2d^2}{M} \sum_{i=1}^{M/2} (2i-1)^2 = \frac{d^2}{3}(M^2-1)$$

$$\therefore \quad P_s = \frac{\overline{a^2}}{T} = \frac{d^2}{T}\,\frac{M^2-1}{3} \quad \Rightarrow \quad d = \sqrt{\frac{3\,P_s\,T}{M^2-1}}$$

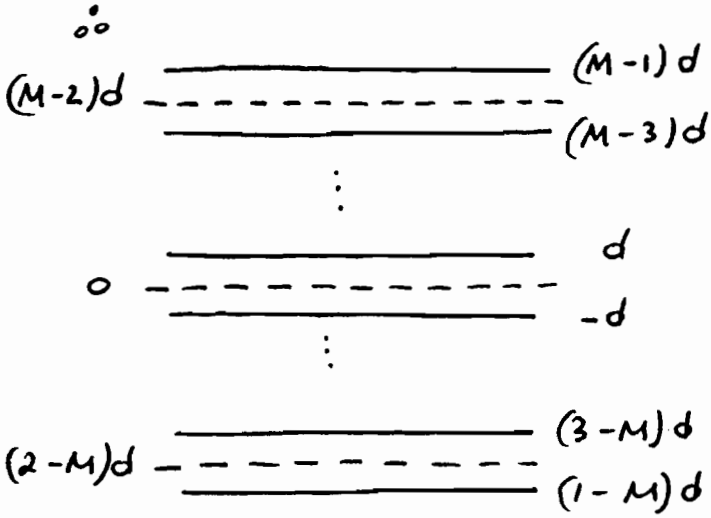

$$P_E = \left(1 - \frac{1}{M}\right) Pr[|n| > d]$$

$P_E = k\, P_e$ (Gray coding)

(8-PAM

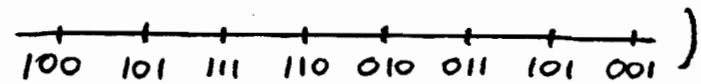

)

The noise at the output of Rx-filter is still Gaussian with power

$$\sigma^2 = \frac{N_0}{2}\int_{-\infty}^{\infty} H(f)\,df = \frac{N_0}{2}$$

$$d = \sqrt{\frac{3 P_s T}{M^2-1}}$$

$$\Rightarrow P_E = 2\left(1-\frac{1}{M}\right) Q\left(\frac{d}{\sigma}\right)$$

$$= 2\left(1-\frac{1}{M}\right) Q\left(\sqrt{\frac{3}{M^2-1}\, 2\, \frac{P_s T}{N_0}}\right)$$

For 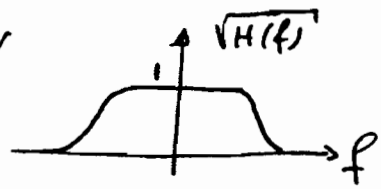

$$\rightarrow \int_{-\infty}^{\infty} H(f)\,df = \frac{1}{T}$$

$\therefore \frac{N_0}{T} \equiv$ noise power $= P_N$

$$\therefore P_E = 2\left(1-\frac{1}{M}\right) Q\left(\sqrt{2}\sqrt{\frac{3}{M^2-1}\,\frac{P_s}{P_N}}\right) = 2\left(1-\frac{1}{M}\right) Q\left(\sqrt{2}\sqrt{\frac{3}{M^2-1}\,\frac{S}{N}}\right)$$

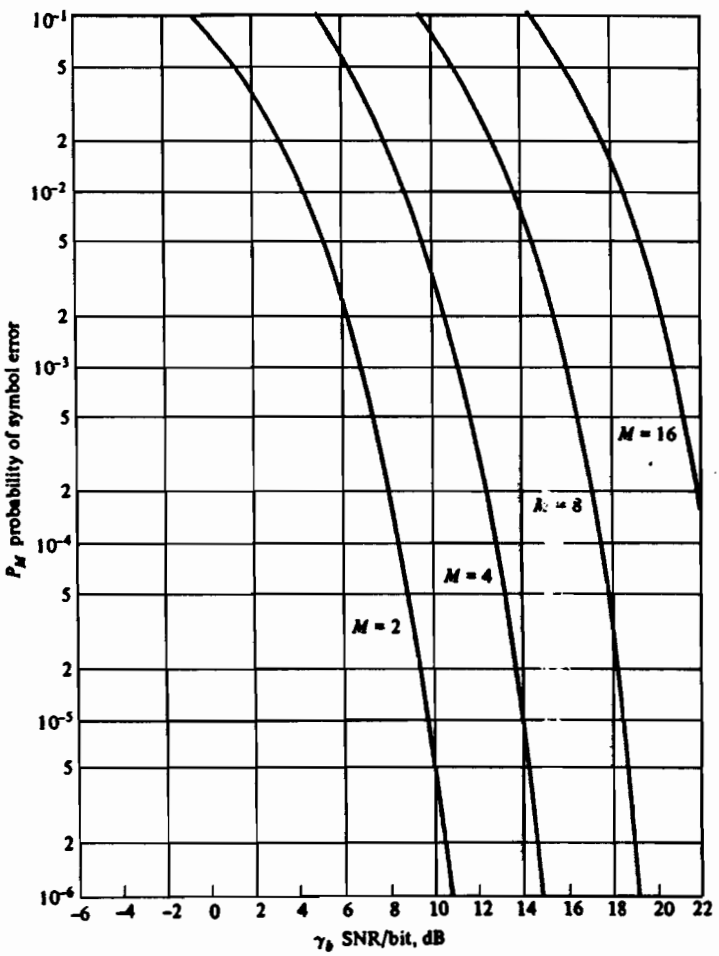

FIGURE 4.2.23
Probability of a symbol error for PAM.

COMBINED AMPLITUDE AND PHASE MODULATIONS

M = 8

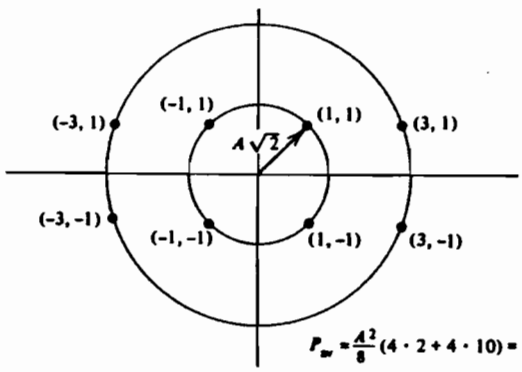

$P_{av} = \frac{A^2}{8}(4 \cdot 2 + 4 \cdot 10) = 6A^2$

(a)

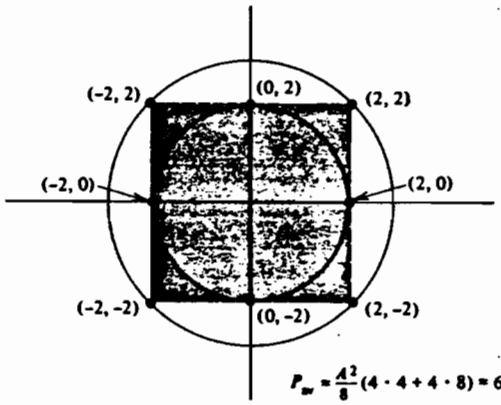

$P_{av} = \frac{A^2}{8}(4 \cdot 4 + 4 \cdot 8) = 6A^2$

(b)

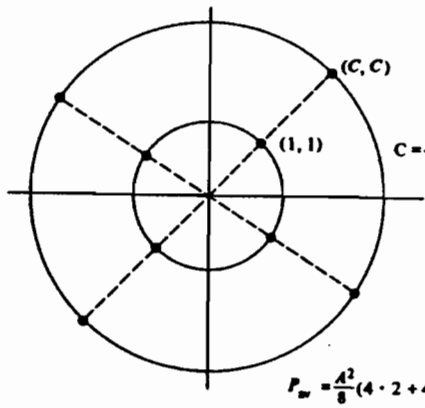

$P_{av} = \frac{A^2}{8}(4 \cdot 2 + 4 \cdot 11.66)$
$= 6.83A^2$

(c)

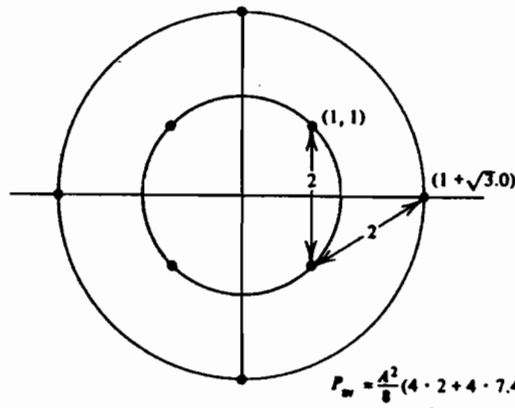

$P_{av} = \frac{A^2}{8}(4 \cdot 2 + 4 \cdot 7.464)$
$= 4.73A^2$

(d)

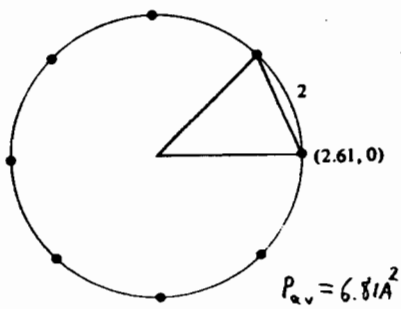

$P_{av} = 6.81A^2$

M-QAM

$2 \times \sqrt{M}$-PAM $\Longrightarrow$ M-QAM

$\therefore$ P_c for an M-QAM is $P_c = (1 - P_{\sqrt{M}})^2$ where $P_{\sqrt{M}}$ is the error probability for an $\sqrt{M}$-PAM with power $\frac{1}{2}$ of the QAM

$\therefore$ $$P_{\sqrt{M}} = 2\left(1 - \frac{1}{\sqrt{M}}\right) Q\left(\sqrt{2}\sqrt{\frac{3}{M-1}\,\frac{1}{2}\,\frac{S}{N}}\right)$$

$$= \frac{\sqrt{M}-1}{\sqrt{M}}\, \operatorname{erfc}\left(\sqrt{\frac{3}{M-1}\,\frac{1}{2}\,\underbrace{\frac{S}{N}}}\right)$$

for the QAM.

$\therefore$ $$P_E = 1 - (1 - P_{\sqrt{M}})^2 \simeq 2 P_{\sqrt{M}}$$

M-PSK

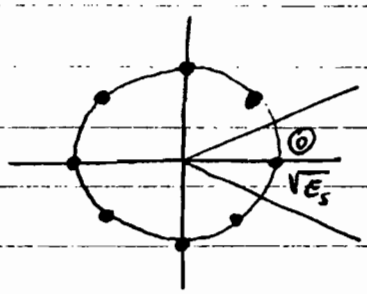

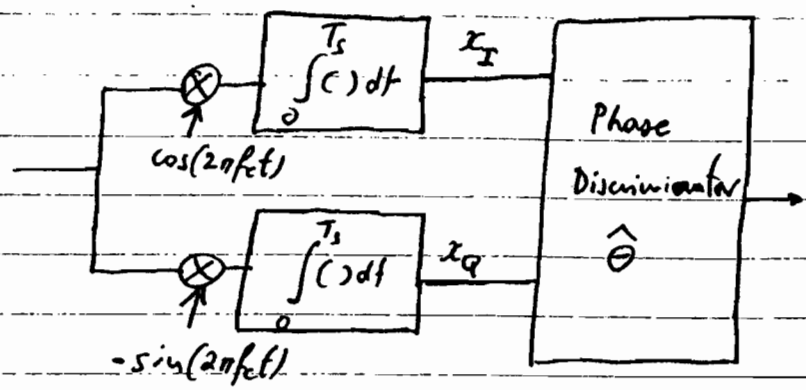

$$x_I(t) = \sqrt{E_s}\cos\left(\frac{2\pi i}{M}\right) + n_I(t)$$

$$x_Q(t) = \sqrt{E_s}\sin\left(\frac{2\pi i}{M}\right) + n_Q(t)$$

independant Grv, zero mean, $\sigma^2 = \frac{N_0}{2}$

Symmetric Constellation $\Rightarrow$ Point ⊙

$$P_c = \int_{-\frac{\pi}{M}}^{\frac{\pi}{M}} f_\Theta(\hat{\theta})\,d\hat{\theta} \quad ; \quad \hat{\theta} = \arctan\left[\frac{n_Q(t)}{\sqrt{E_s} + n_I(t)}\right]$$

($\equiv$ phase of a sine wave plus narrow band noise)

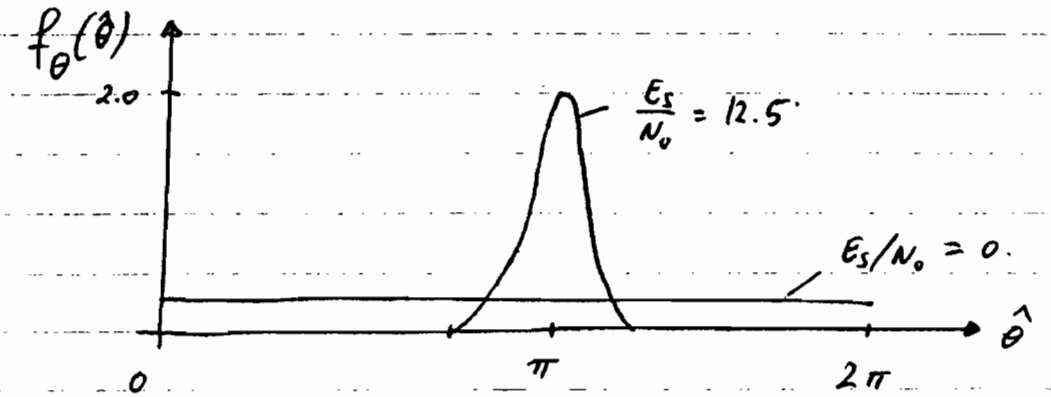

$$P_E = 1 - P_c \simeq \dots \simeq \operatorname{erfc}\left[\sqrt{\frac{E_s}{N_0}}\sin\left(\frac{\pi}{M}\right)\right]$$

Approximation tighter $M \uparrow$ and $\frac{E_s}{N_0} \uparrow$

Some Comparisons

M-PSK

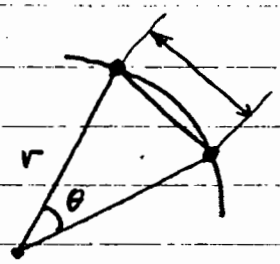

$$\left.\begin{aligned} \theta &= \frac{2\pi}{M} \\ \sin\left(\frac{\theta}{2}\right) &= \frac{1}{r} \end{aligned}\right\} \Rightarrow r \simeq \frac{M}{\pi} \text{ for } M \uparrow.$$

$\therefore$ P_{av} increases by $\left(\frac{M}{\pi}\right)^2$ as M increases.

For QAM: " " - $\frac{2(M-1)}{3}$ " " -

$$\therefore D_M = \frac{3M^2}{2(M-1)\pi^2}$$

$M = 8 \Rightarrow$ 1.43 dB (QAM is better than PSK)

$M = 64 \Rightarrow$ 9.95 dB (" - - - -)

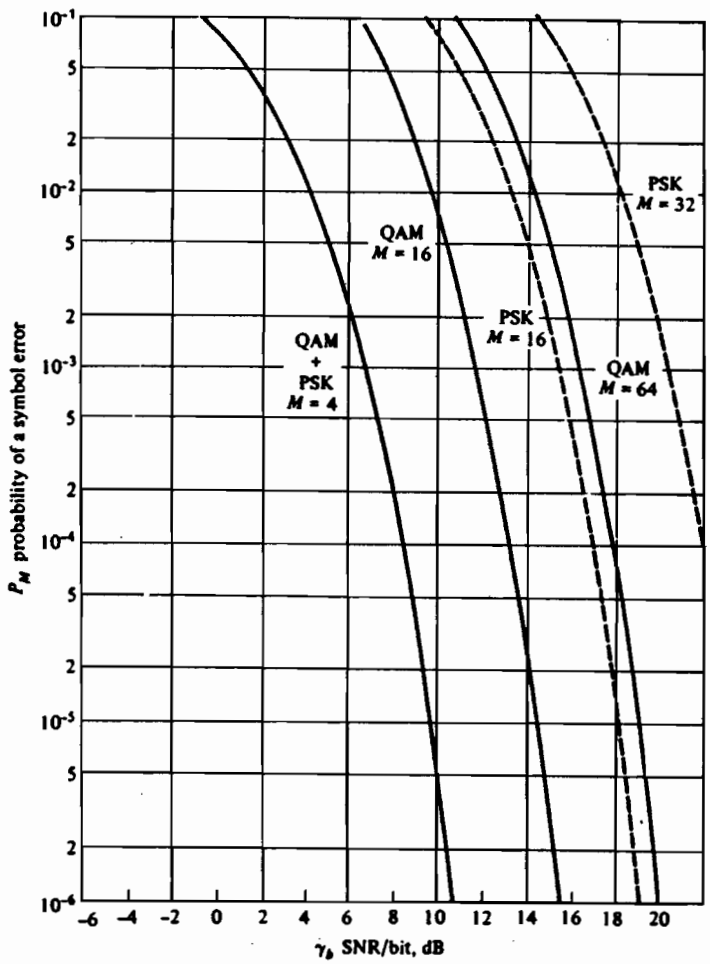

FIGURE 4.2.28
Probability of a symbol error for QAM and PSK.

DIFFERENTIALLY ENCODED AND DIFFERENTIALLY DETECTED (COHERENT) PSK SIGNALS

- Coherent systems exibit a phase ambiguity

e.g.,

$$a_k \cos(2\pi f_c t) \xrightarrow{(\cdot)^2} \cos^2(2\pi f_c t) = \frac{1}{2} + \frac{1}{2}\cos(4\pi f_c t)$$

$a_k \in \{\pm 1\}$

$$\therefore \cos(4\pi f_c t) \xrightarrow[\text{by } 2]{\text{freq. div.}} \begin{cases} \cos(2\pi f_c t + 180^\circ) \\ \cos(2\pi f_c t + 0^\circ) \end{cases} \quad \underline{\text{which one?}}$$

$-\ +360^\circ$
$-\ +0^\circ$

- M-DPSK (Differentially encoded PSK)

$\theta_n = \theta_{n-1} + \frac{2\pi}{M} a_n$; θ_n carrier phase at $t = nT$
a_n data symbol " "

$M = 4 \rightarrow \left\{ \lambda, \lambda + \frac{\pi}{2}, \lambda + \pi, \lambda + \frac{3\pi}{2} \right\}$

$\underline{\lambda = 0}$

(DQPSK)

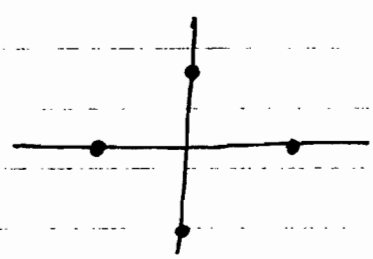

$\underline{\lambda = \frac{\pi}{4}}$

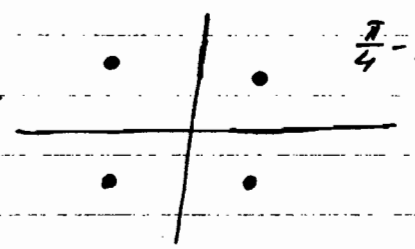

$\frac{\pi}{4}$-DQPSK

$$t = nT \Rightarrow V_n = E_s e^{j(\theta_n - \varphi)} + N_n$$

$$t = (n-1)T \Rightarrow V_{n-1} = E_s e^{j(\theta_{n-1} - \varphi)} + N_{n-1}$$

The decision variable is the phase of the product $V_n V_{n-1}^*$

$$U_n = V_n V_{n-1}^* = E_s^2 e^{j(\theta_n - \theta_{n-1})} + E_s N_n e^{-j(\theta_{n-1} - \varphi)} + E_s N_{n-1}^* e^{j(\theta_n - \varphi)} + N_n N_{n-1}^*$$

Without noise $\Rightarrow \therefore \theta_n - \theta_{n-1}$ (the desired).

i) DBPSK (Binary) $\Rightarrow$ Real signals

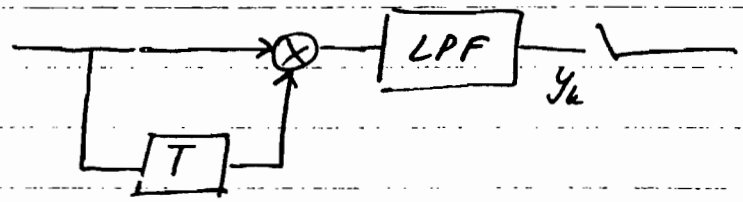

$t = nT \Rightarrow \cos(2\pi f_c t + \theta_n + \varphi)$ $\quad \theta_n \in \{0, \pi\}$

$t = (n-1)T \Rightarrow \cos(2\pi f_c t + \theta_{n-1} + \varphi)$

$\therefore y_k \sim \cos(\theta_n - \theta_{n-1})$

ii) DQPSK

$$U_n = E_s + (N_n + N_{n-1}^*) + N_n N_{n-1}^*$$

(delete E_s & the noise terms include the $e^{-j(\cdot)}$).

$N_n N_{n-1}^*$ small

$$\therefore \quad U_n' = E_s + N_n + N_{n-1}^* = X + jY$$

$$X = E_s + Re[N_n + N_{n-1}^*]$$

$$Y = Im[N_n + N_{n-1}^*]$$

N_n, N_{n-1}^* uncorrelated Grv

$\sigma^2 = \frac{N_0}{2}$

$$\therefore \quad \theta_i = \arctan \frac{X}{Y}$$

Identical problem with the coherent PSK. However, the noise is twice as much

$\therefore$ we except a degradation of 3 dB as compared to coherent QPSK.

It turns out that for DBPSK this degradation is less

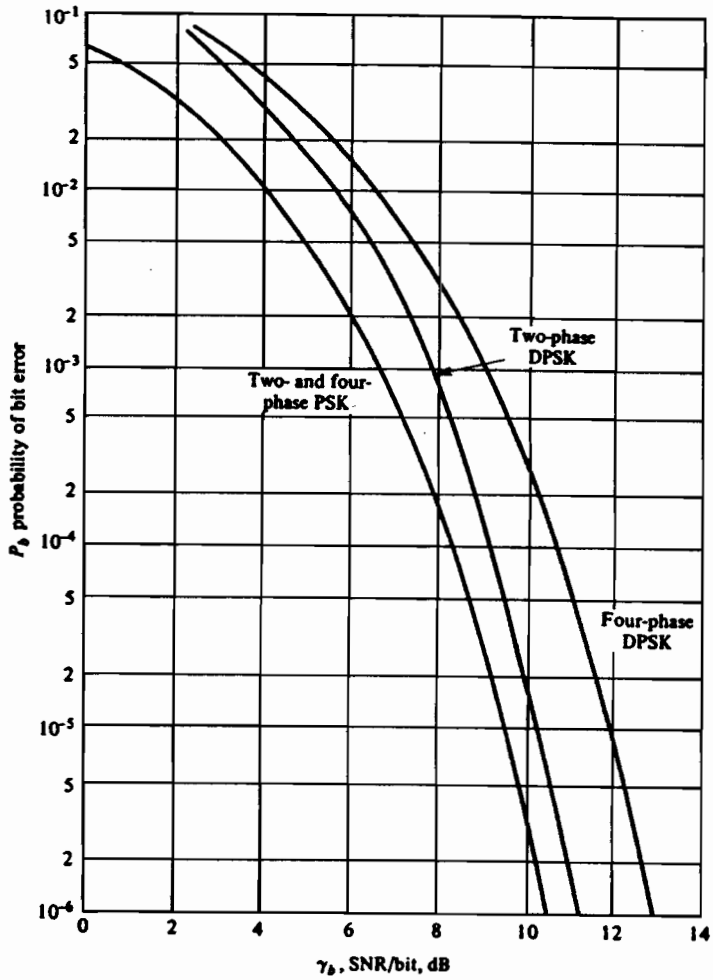

FIGURE 4.2.20
Probability of bit error for binary and four-phase PSK and DPSK.

PARTIAL RESPONSE SYSTEMS

- Filter here are chosen so that they <u>don't</u> satisfy Nyquist but they result in a controlled amount of ISI. ⇒ Can be removed at the Rx.

1) Duobinary PR

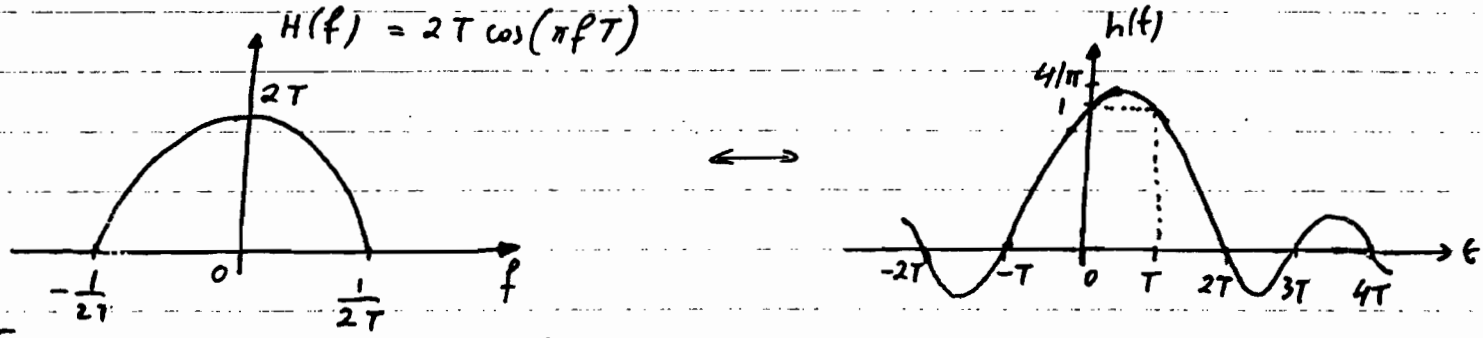

[Filter design: Analog or Digital

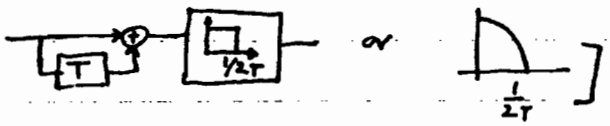

]

$$h(nT) = \begin{cases} 1, & n = 0, 1 \\ 0 & \text{otherwise} \end{cases}$$

<u>No noise</u>

Received signal $r(t) = \sum_k a_k h(t - nT)$; $a_k \in \{\pm d\}$

$$r(nT) = a_n + a_{n-1} = \begin{cases} 2d \\ 0 \\ -2d \end{cases}$$

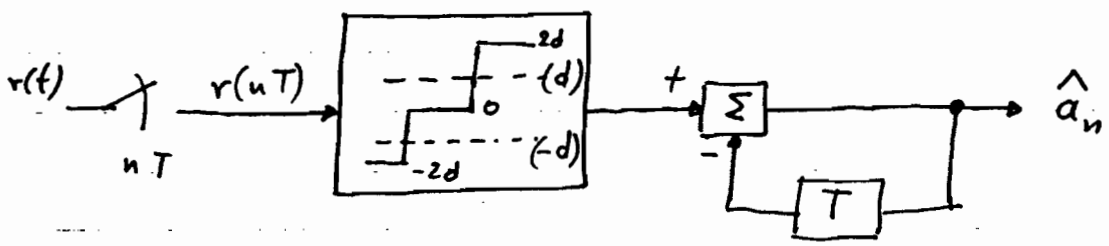

With noise ⇒ Errors occur when

$N_n > d$ for $+2d$

$N_n < -d$ for $-2d$

$|N_n| > d$ for 0

Because of the decision feedback ⇒ error propagation

∴ Precoding (similar to differential encoding)

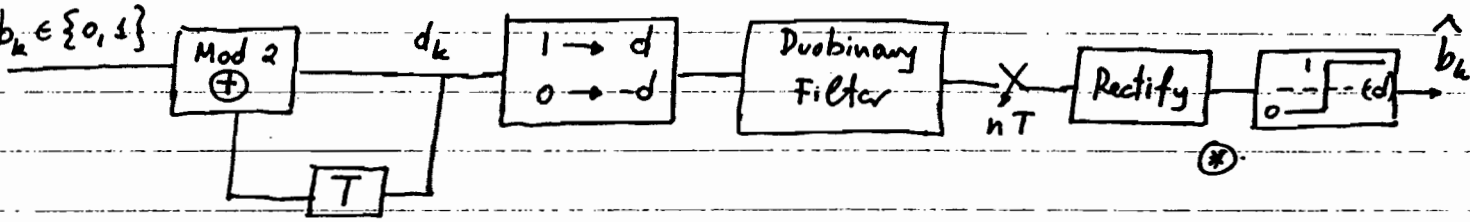

* If $d_k \neq d_{k-1}$ (0 received) ⇒ $b_k = 1$

If $d_k = d_{k-1}$ ($\pm 2d$ u) ⇒ $b_k = 0$

For <u>optimum</u> split of the Duobinary filter, i.e.,

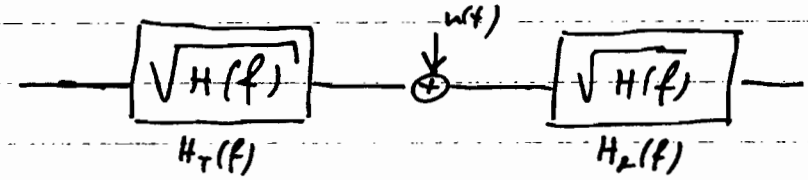

$$Pr[\text{error}] = \frac{1}{4} Pr(N \leq -d) + \frac{1}{2} Pr(|N| \geq d) + \frac{1}{4} Pr(N \geq d)$$

$$= \frac{3}{2} Q\left(\frac{d}{\sigma_N}\right)$$

$$P_s = \frac{d^2}{T} \int_{-\infty}^{\infty} |H_T(f)|^2 df$$

$$\sigma_N^2 = \frac{N_0}{2} \int |H_R(f)|^2 df$$

∴ $$P = \frac{3}{2} Q\left[\sqrt{\frac{2P_s T}{N_0}} \frac{\pi}{4}\right]$$ ⇒ requires 2.1 dB more than the Nyquist 2-PAM!!

For an L-level duobinary system

$$P_\varepsilon = 2\left(1 - \frac{1}{L^2}\right) Q\left[\sqrt{\frac{3 P_s T}{(L^2-1) N_0}\left(\frac{\pi}{4}\right)}\right]$$

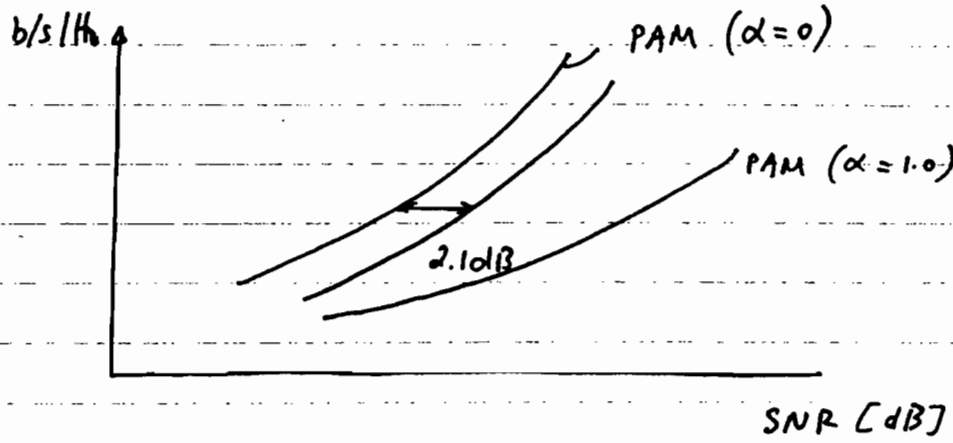

2) Modified Duobinary PR (class IV)

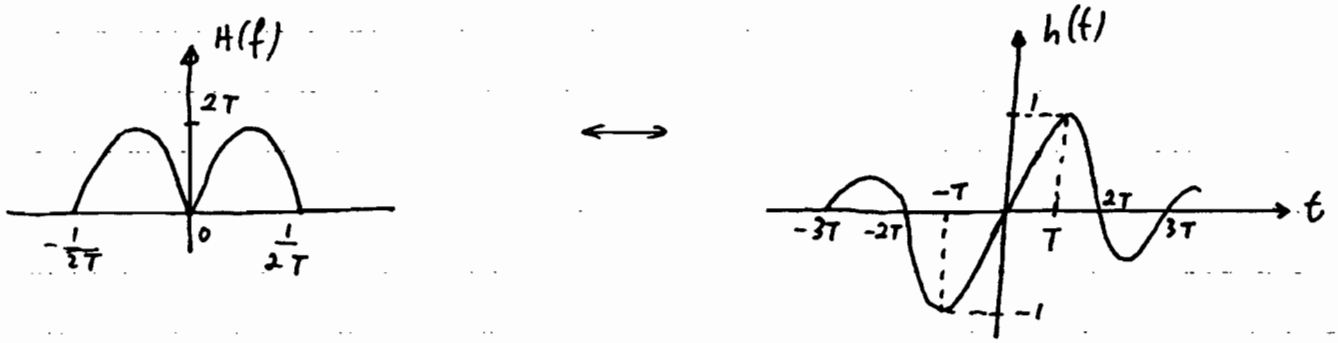

Some performance as Duobinary. (Precoding : 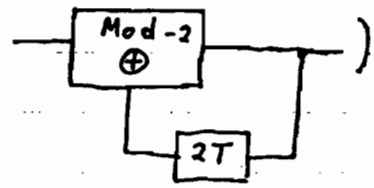

)

Spectrum different

Comments

① PR → minimum bandwidth ; "easy" filters

② 2.1 dB loss for "simple" receivers. With Viterbi receives we can get this loss back.

COHERENT SYSTEMS

- AWGN
  1) Square law carrier recovery
  2) Costas loop
  3) M-th law carrier recovery

- Fading
  1) Pilot Tones
  2) Pilot Sequences

I) Square-law carrier recovery

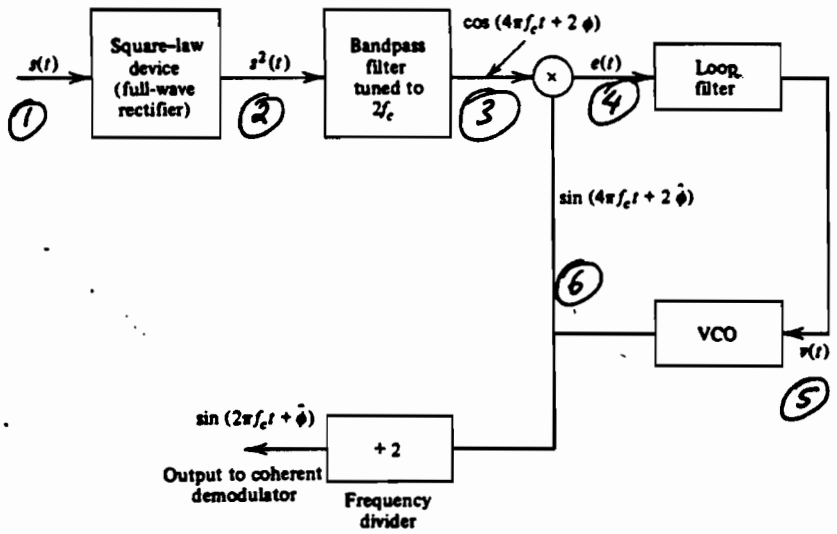

① $s(t) = A(t)\cos(2\pi f_c t + \phi)$

② $s^2(t) = A^2(t)\cos^2(2\pi f_c t + \phi) = \frac{1}{2}A^2(t) + \frac{1}{2}A^2(t)\cos(4\pi f_c t + 2\phi)$

③

④ Error signal: $e(t) = \cos(4\pi f_c t + 2\phi)\sin(4\pi f_c t + 2\hat{\phi})$
$= \frac{1}{2}\sin[2(\phi + \hat{\phi})] + \frac{1}{2}\sin(8\pi f_c t + 2\phi + 2\hat{\phi})$

⑤ $v(t) = \frac{1}{2}\sin[2(\phi + \hat{\phi})]$

⑥ Instantaneous phase of the sinusoid:

$$4\pi f_c t + 2\hat{\phi}(t) = 4\pi f_c t + K\int_{-\infty}^{t} v(z)\,dz$$

$$\therefore \quad 2\hat{\phi} = K\int_{-\infty}^{t} v(z)\,dz$$

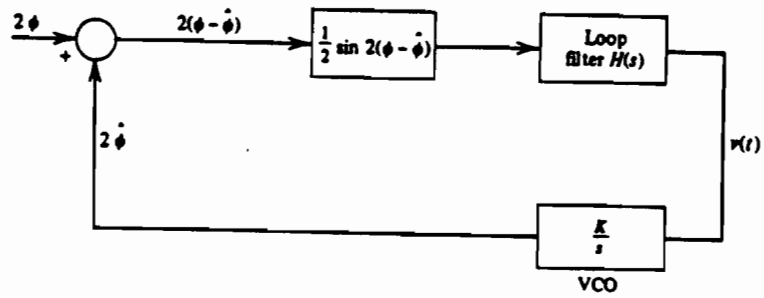

Model of the phase-locked loop.

Simplification when phase error is small

$$\frac{1}{2}\sin[2(\phi-\hat{\phi})] \simeq \phi-\hat{\phi}$$

Linear analysis $\Longrightarrow$ <u>without sin( )</u>

To include the AWGN, $n(t)$

$$n(t) = x(t)\cos(2\pi f_c t) - y(t)\sin(2\pi f_c t)$$

$$s(t) = A_c \cos[2\pi f_c t + \phi(t)].$$

It's convenient to rewrite $n(t)$ as

$$n(t) = n_c(t)\cos[2\pi f_c t + \phi(t)] - n_s(t)\sin[2\pi f_c t + \phi(t)]$$

$$n_c(t) = x(t)\cos[\phi(t)] + y(t)\sin[\phi(t)]$$
$$n_s(t) = -x(t)\sin[\phi(t)] + y(t)\cos[\phi(t)]$$

$$\left\{ n_c(t) + j n_s(t) = [x(t) + j y(t)] e^{-j\phi(t)} \right\}$$

Note: $n_c(t)$ & $n_s(t)$ have the same statistical characteristics as $x(t)$ & $y(t)$.

Now $s(t) + n(t)$ is multiplied by the output of the VCO $\longrightarrow$ after LPF we get.

$$e(t) = A_c \sin(\Delta\phi) + n_c(t)\sin(\Delta\phi) - n_s(t)\cos(\Delta\phi)$$
$$= A_c \sin(\Delta\phi) + n_1(t)$$

where $\Delta\phi = \phi - \hat{\phi}$

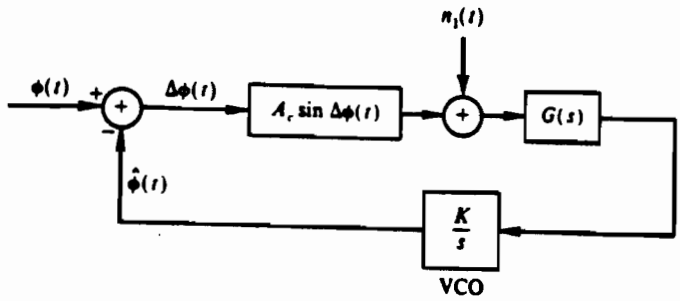

PLL model with AWGN

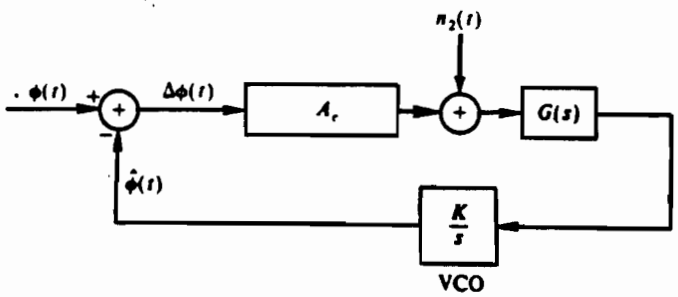

"Linearized model" → $(A_c^2/2 \gg$ Noise power$)$.

$$\left\{ n_2(t) = \frac{n_c(t)}{A_c} \sin(\Delta\phi) - \frac{n_c(t)}{A_c} \cos(\Delta\phi) \right\}$$

Note: $n_2(t)$ additive → $\sigma_{\Delta\phi}^2 = \frac{2 N_0 B_{eq}}{A_c^2}$

$B_{eq} \triangleq$ equivalent noise bandwidth of the loop.

∴ SNR $\triangleq \gamma_L = \frac{A_c^2/2}{N_0 B_{eq}}$ || Valid only for "linearized" model

For exact analysis $\Longrightarrow$ very complicated.

$$G(s) = 1. \longrightarrow p(\Delta\phi) = \frac{\exp(\gamma_L \cos\Delta\phi)}{2\pi I_0(\gamma_L)}$$

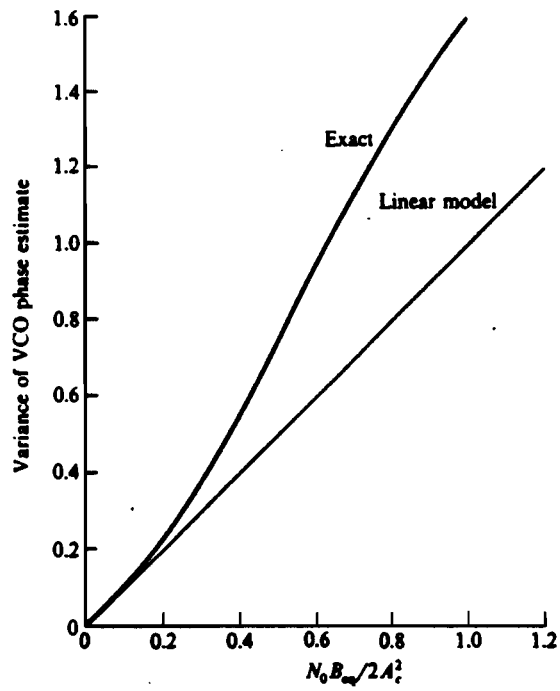

Noise Enhancement due to the Nonlinear Operation.

$$[s(t) + n(t)] \xrightarrow{(\,)^2} \underbrace{s^2(t)}_{\text{signal}} + \underbrace{2s(t)n(t)}_{\text{signal} \times \text{noise}} + \underbrace{n^2(t)}_{\text{noise} \times \text{noise}}$$

∴ Additional noise !!

Since $B_{bpf} \gg B_{eq}$ (of PLL) $\Rightarrow$ noise within PLL is constant.

$$\sigma_{\Delta\phi}^2 = \frac{1}{\gamma_L S_L}$$

$S_L \triangleq$ squaring loss $= \dfrac{1}{1 + \dfrac{B_{bpf}/2B_{eq}}{\gamma_L}}$

- $S_L < 1$
- S_L^{-1} represents the increase in the variance of the phase error caused by the added noise $n(t)$ (noise × noise term)

  Example: $\gamma_L = B_{bpf}/2B_{eq}$ $\rightarrow$ loss is 3dB.
- Freq. division by 2 $\Rightarrow$ phase ambiguity of 180°.

  Solution: Differential Encoding.

II) Costas Loop

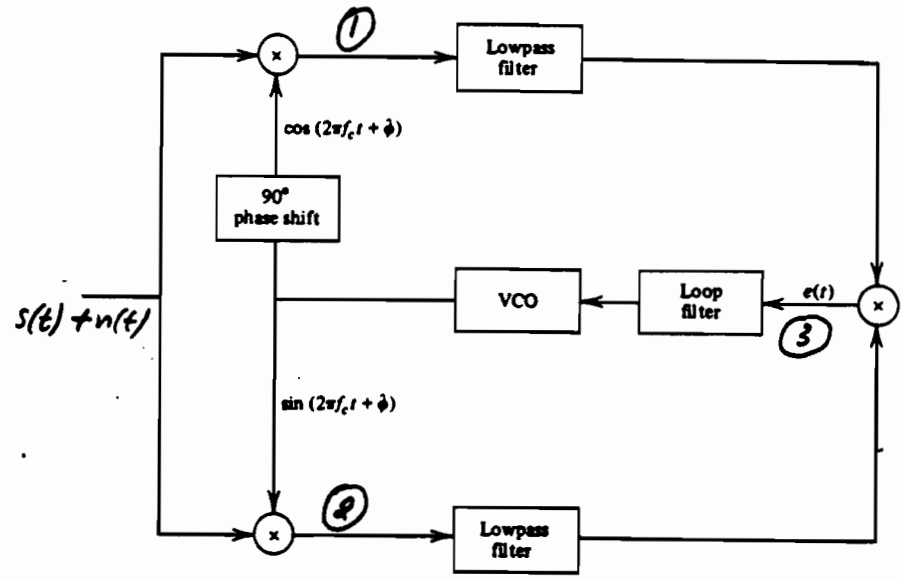

① : $[s(t) + n(t)] \cos(2\pi f_c t + \hat{\phi})$

$= \frac{1}{2}[A(t) + n_c(t)] \cos(\Delta\phi) + \frac{1}{2} n_s(t) \sin(\Delta\phi) + \left\{ \begin{matrix} \text{Double} \\ \text{Frequency} \\ \text{Terms} \end{matrix} \right\}$

② : $[s(t) + n(t)] \sin(2\pi f_c t + \hat{\phi})$

$= \frac{1}{2}[A(t) + n_c(t)] \sin(\Delta\phi) - \frac{1}{2} n_s(t) \cos(\Delta\phi) + \left\{ \begin{matrix} \text{Double} \\ \text{Frequency} \\ \text{Terms} \end{matrix} \right\}$

$\Delta\phi \triangleq \phi - \hat{\phi}$

③ : $e(t) = \frac{1}{8}\left\{[A(t) + n_c(t)]^2 - n_s^2(t)\right\} \sin(2\Delta\phi)$

$- \frac{1}{4} n_s(t)[A(t) + n_c(t)] \cos(2\Delta\phi)$

Desired term: $A^2(t) \sin(2\Delta\phi)$

→ signal × noise

→ noise × noise

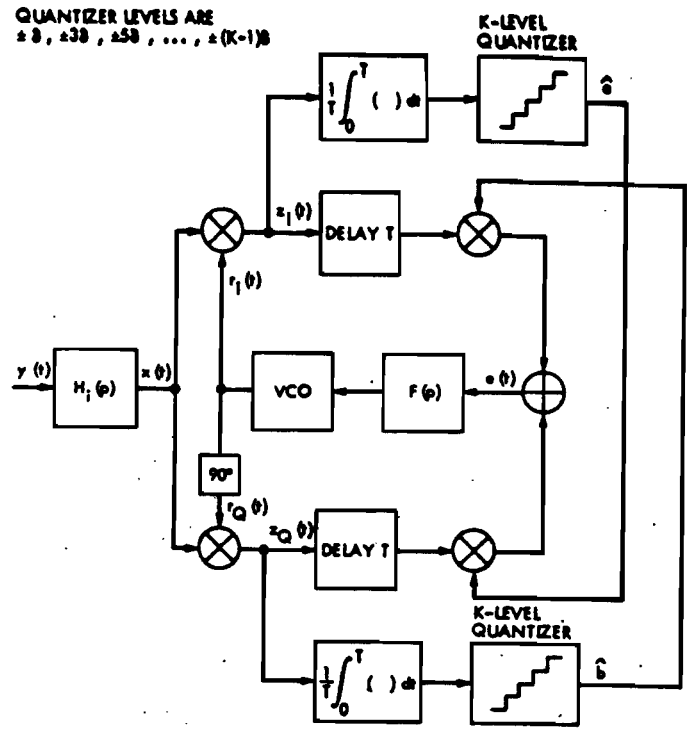

Fig. 3. Carrier reconstruction loop for QASK signals.

Simon & Smith, "Carrier synchronization and detection for QASK signal sets," IEEE Trans. Com., Feb. 1974

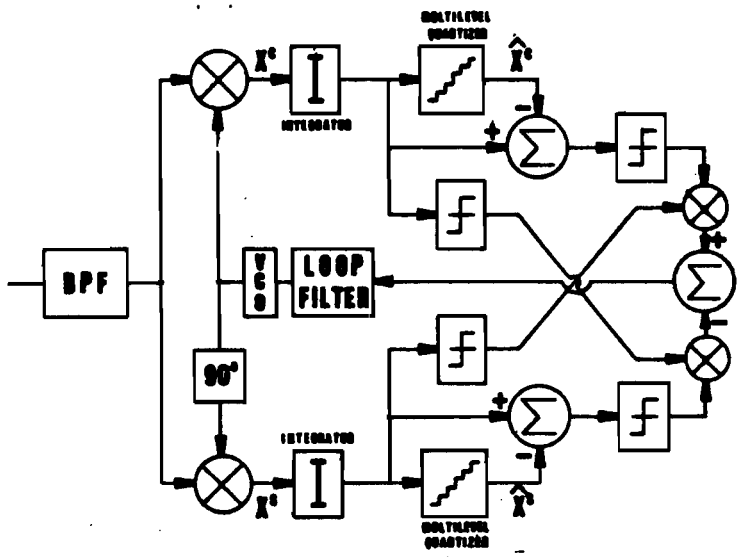

Fig. 2. Proposed carrier recovery loop diagram.

Ref. A. Leclert & P. Vandamme, "Universal Carrier Recovery Loop for QASK and PSK Signal Sets," IEEE Trans. Com., Jan. 1983

III. M-th Power Law. Carrier Recovery.

- M-ary PSK signals

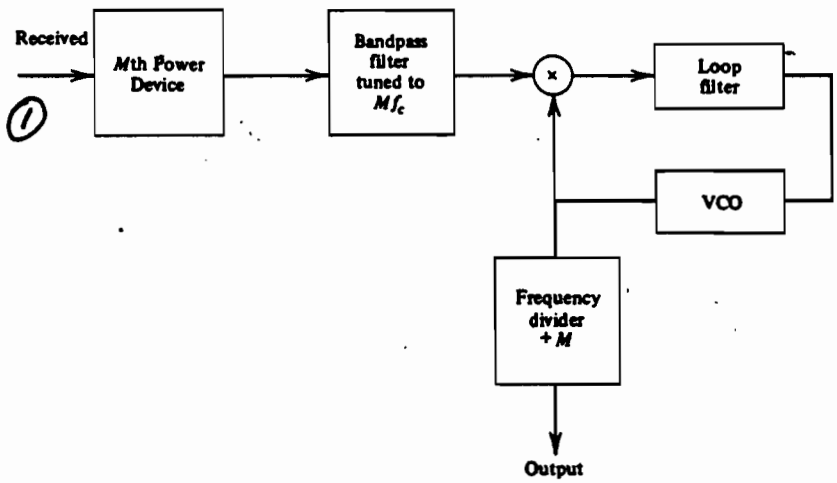

① : $s(t) + n(t)$

② : $[s(t) + n(t)]^M$

$$\sigma^2_{\Delta\phi} = \frac{1}{\gamma_L \, S_{ML}}$$

FADING INTERFERENCE

I) Pilot Tones

- Employ a pilot tone signal ($p(t) = A_p \cos \omega_p t$) to estimate the fading interference.
- Assuming that the fading interference is the same at both the digital signal and the pilot tone $\Rightarrow$ At the receiver we can "undo" the effects of fading.

- Disadvantages:
  - i) Additional power to the pilot(s)
  - ii) Additional bandwidth required for the pilot(s) signals.

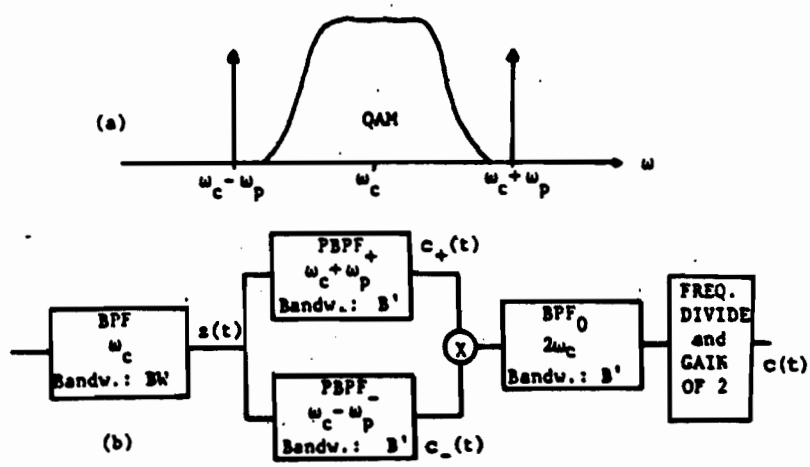

Fig. 1 (a) Transmitted Dual Pilot System (DPS) signal power spectrum.
(b) DPS carrier extraction subsystem used for BPSK (Ref. [10]) as well as for more spectrally efficient systems, such as 16-QAM, 64-QAM,... .

Ref.

Mathiopoulos & Feher, "Pilot aided techniques for system coherent phase jitter cancellation," IEEE Trans. Broadcasting, pp. 356-366, Sept. 1988

IEEE TRANSACTIONS ON COMMUNICATIONS, VOL. COM-32, NO. 1, JANUARY 1984

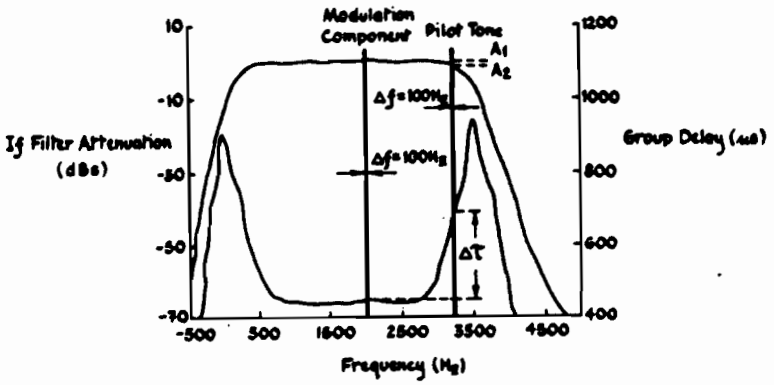

Fig. 1. Typical IF crystal filter characteristic for 5 kHz channel spacing.

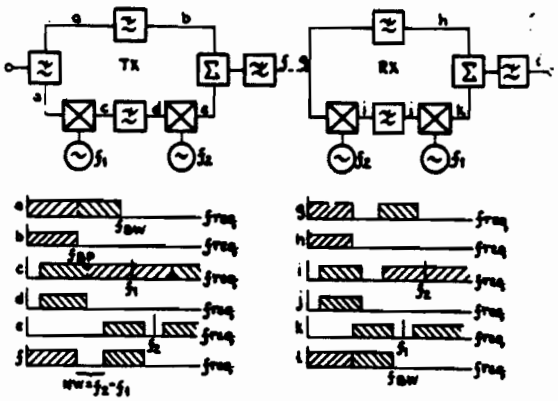

Fig. 2. General implementation of transparent tone-in-band (TTIB).

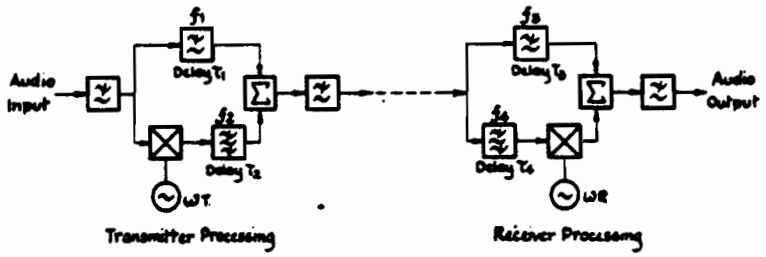

Fig. 3. Experimental TTIB system.

Ref. McGeehan & Bateman
"Phase-locked transparent tone-in-band (TTIB): A new spectrum configuration particularly suited to the transmission of data over SSB mobile networks"

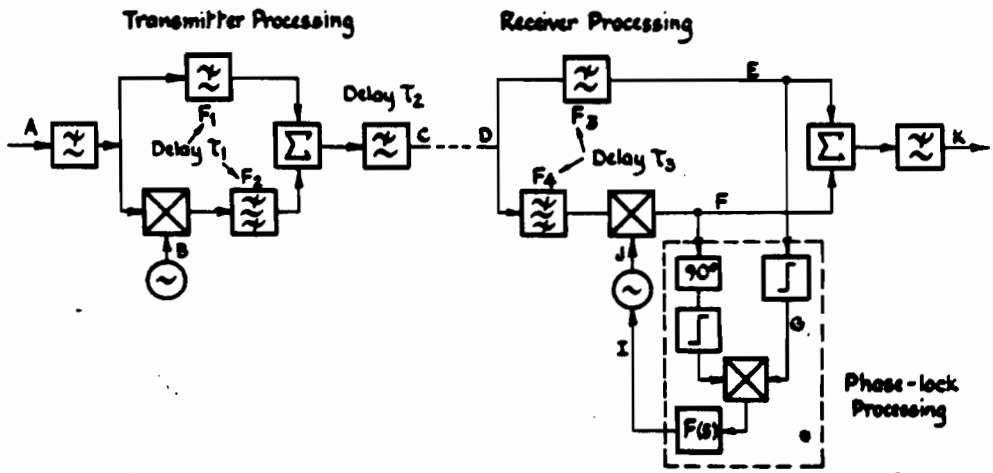

Fig. 4. Phase-locked TTIB processing.

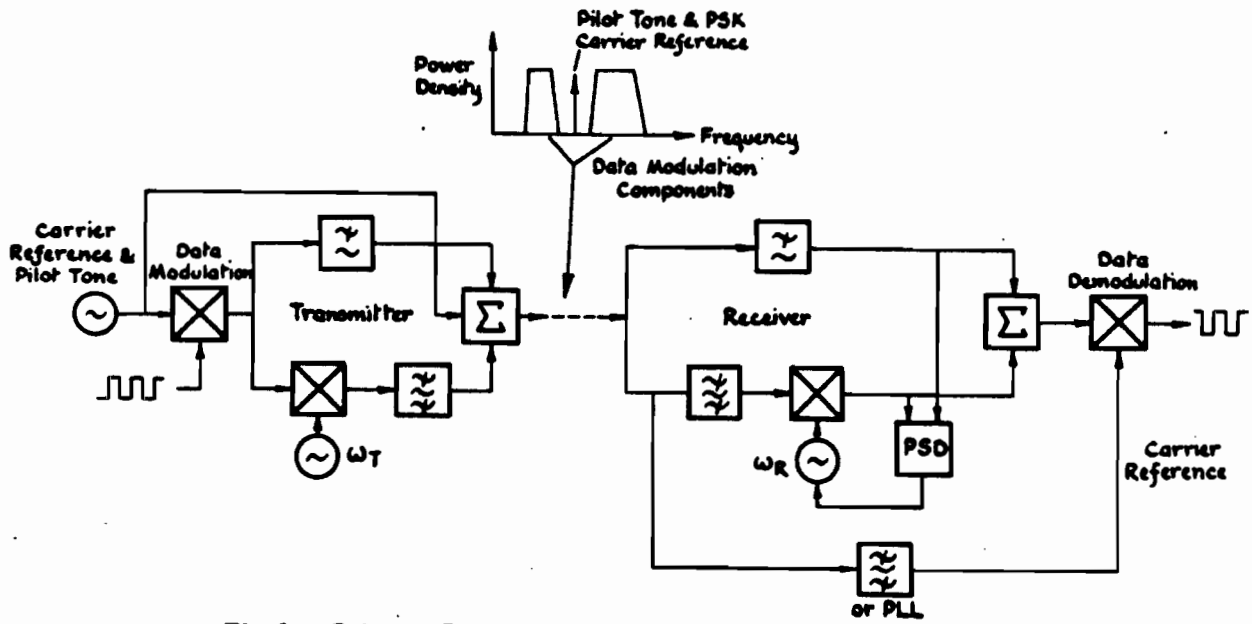

Fig. 9. Coherent PSK data system incorporating TTIB processing.

F. Davarian, "Mobile digital communications via tone calibration," IEEE Trans. Veh. Techn., May 1987 (120)

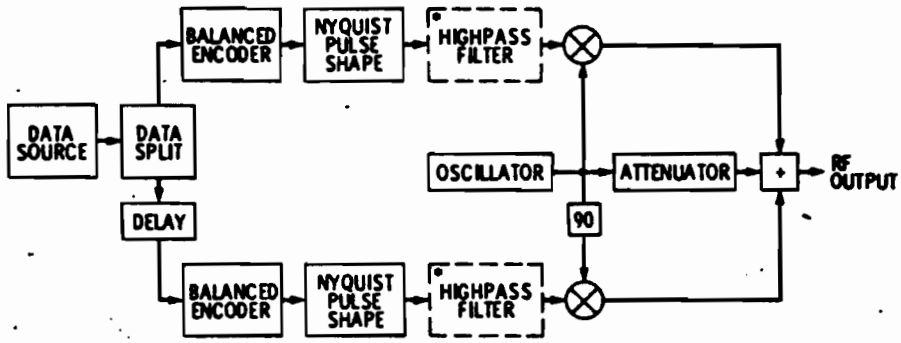

*this filter may be used to reduce self-interference

Fig. 1. The transmitter block diagram.

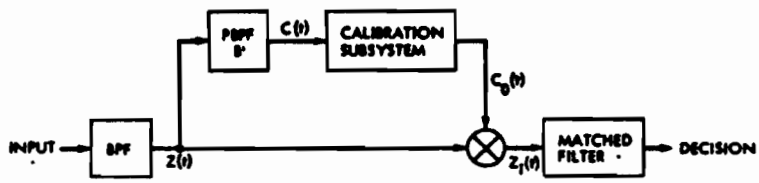

Fig. 2. Receiver block diagram for the in-phase signal component.

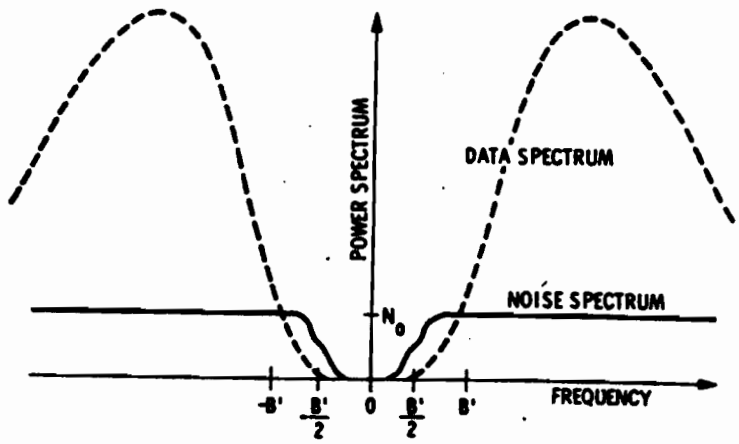

Fig. 3. The power spectral density of noise $N(t)$.

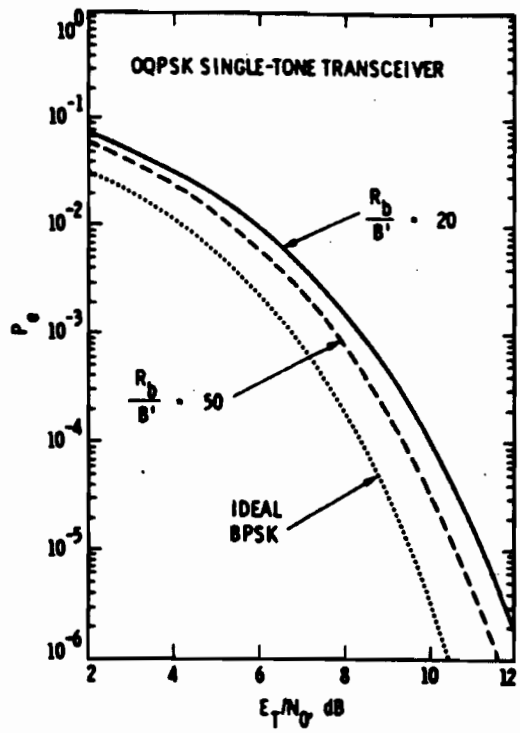

Fig. 5. The receiver error probability in the presence of thermal noise.

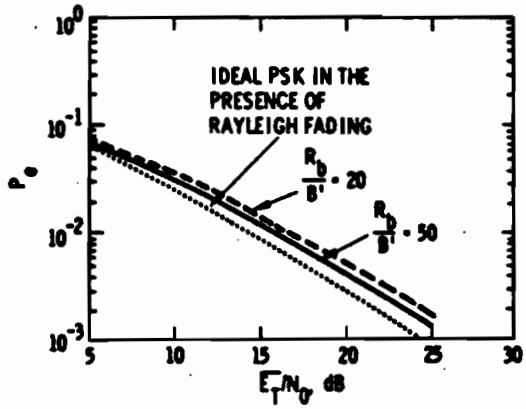

Fig. 6. Receiver performance in the presence of Rayleigh fading.

Ref. M. K. Simon, "Dual-tone pilot calibration technique" IEEE Trans. Veh. Techn., May 1986.

(122)

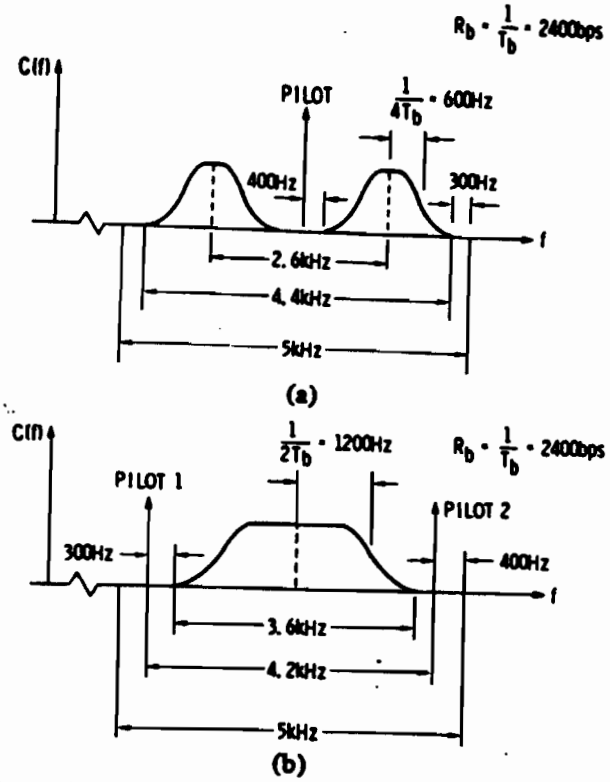

Fig. 1. Composite data and pilot spectra. (a) For 2.4 kbit/s single-pilot TCT; 50-percent excess Nyquist raised cosine QPSK signaling. (b) For 2.4 kbit/s dual-pilot TCT; 50-percent excess Nyquist raised cosine BPSK signaling.

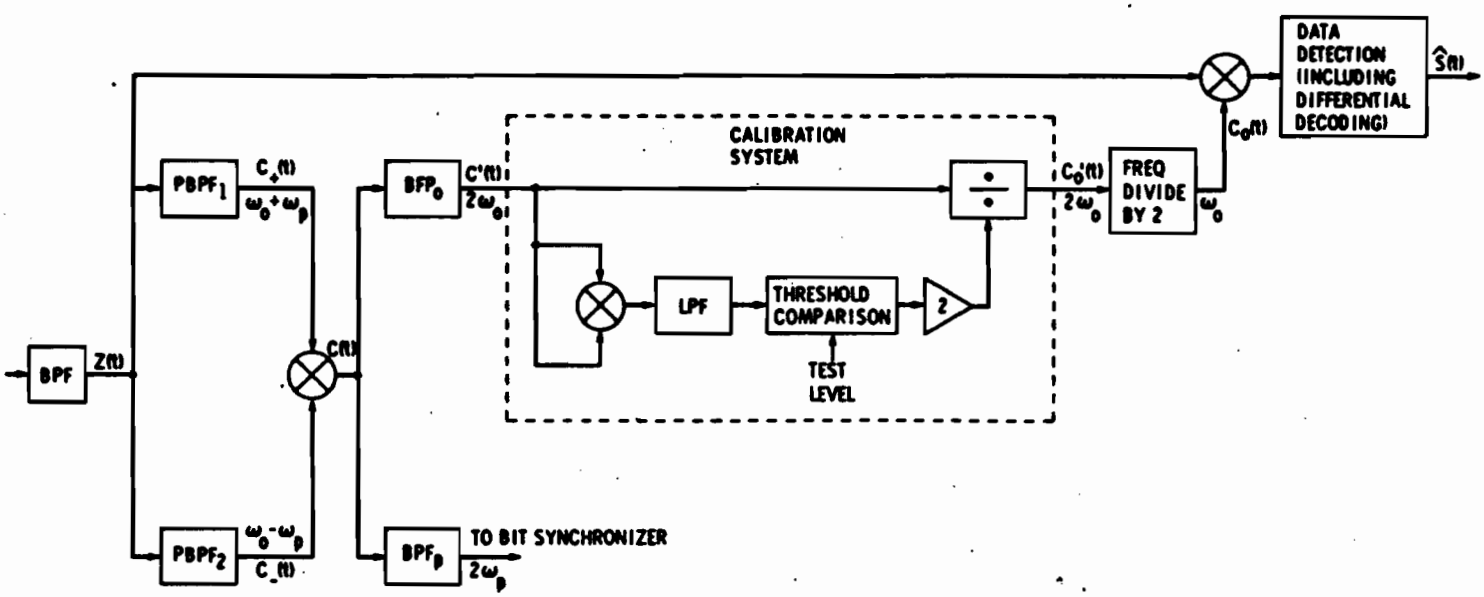

Fig. 2. Dual-pilot TCT receiver, bandpass implementation.

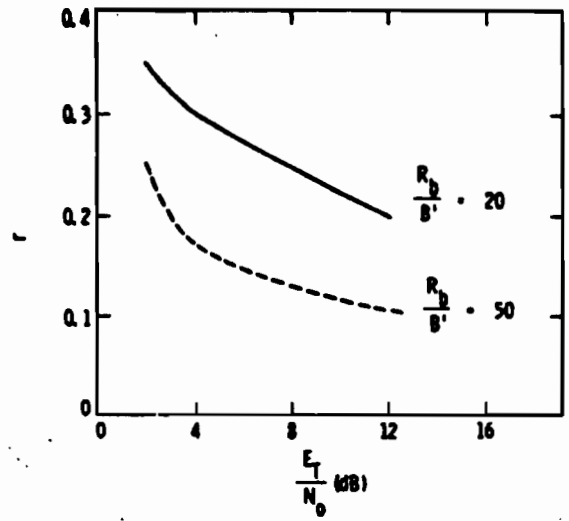

BPSK DOUBLE-TONE TRANSCEIVER

Fig. 3. Ratio of pilot tone to data signal power versus total energy per bit-to-noise ratio with ratio of bit rate to pilot tone BPF bandwidth as parameter; BPSK double-tone transceiver.

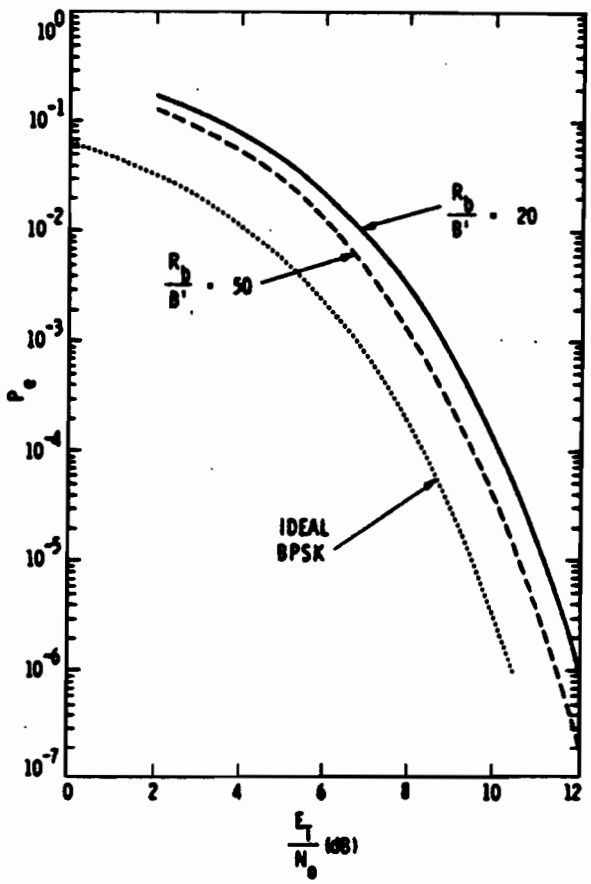

Fig. 4. Bit error probability versus total energy per bit-to-noise ratio with ratio of bit rate to pilot tone BPF bandwidth as parameter; BPSK double-tone transceiver.

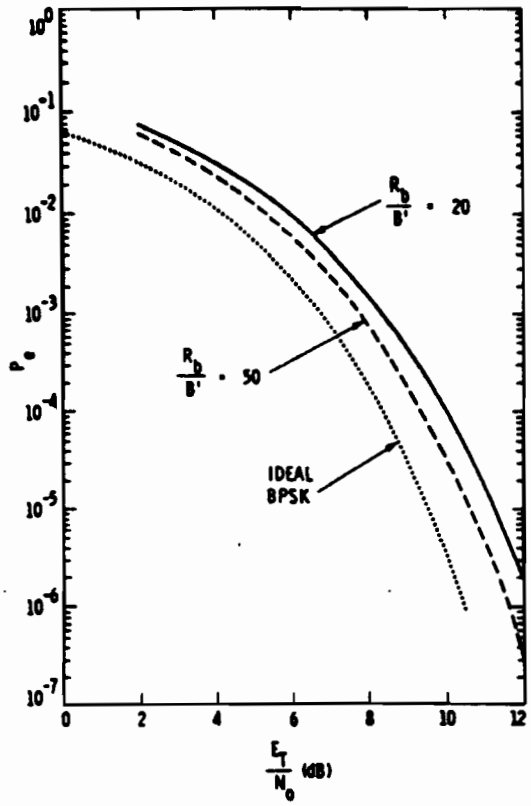

Fig. 6. Bit error probability versus total energy per bit-to-noise ratio with ratio of bit rate to pilot tone BPF bandwidth as parameter; OQPSK single-tone transceiver.

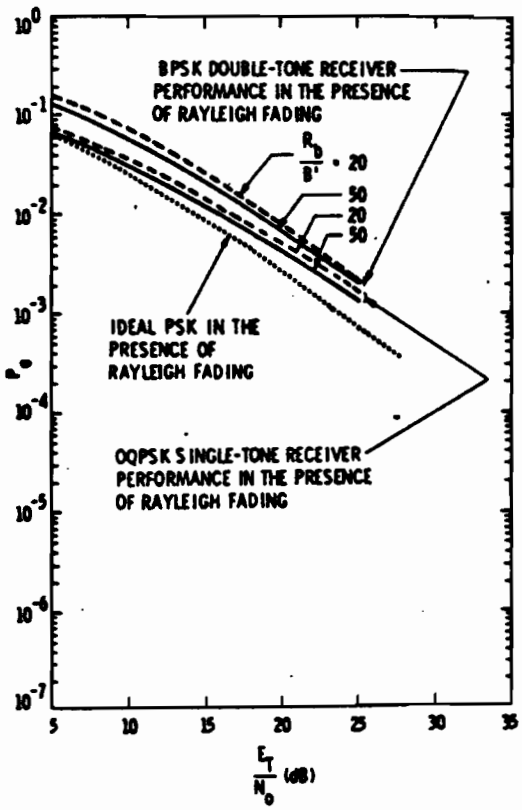

Fig. 7. Bit error probability performances of BPSK double-tone transceiver and OQPSK single-tone transceiver in presence of Rayleigh fading with ratio of bit rate to pilot tone BPF bandwidth as parameter.

Matthiopoulos & Feher, "Pilot aided techniques for System caused phase jitter cancellation," IEEE Trans. Broadcasting, Sept. 1988 [R-2]

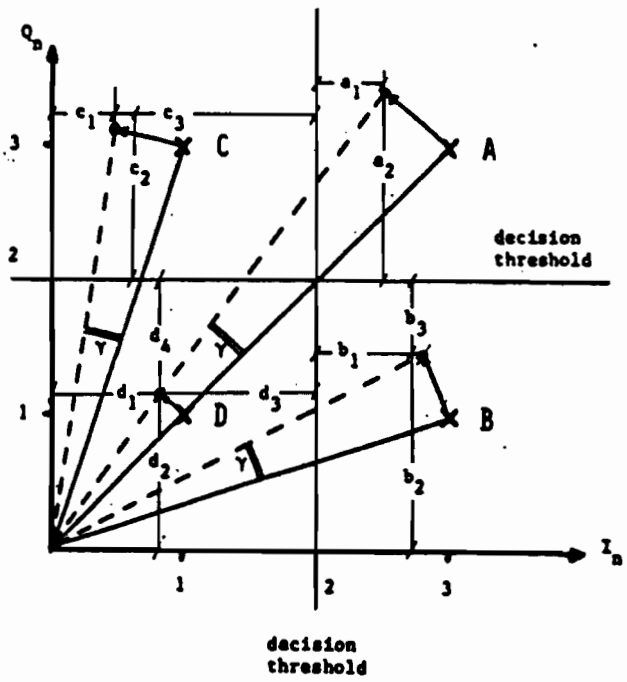

Fig. 3 Signal constallation changes of a 16-QAM system, which is corrupted by system caused phase jitter γ. Due to symmetry, only the points of the first quadrant are shown.

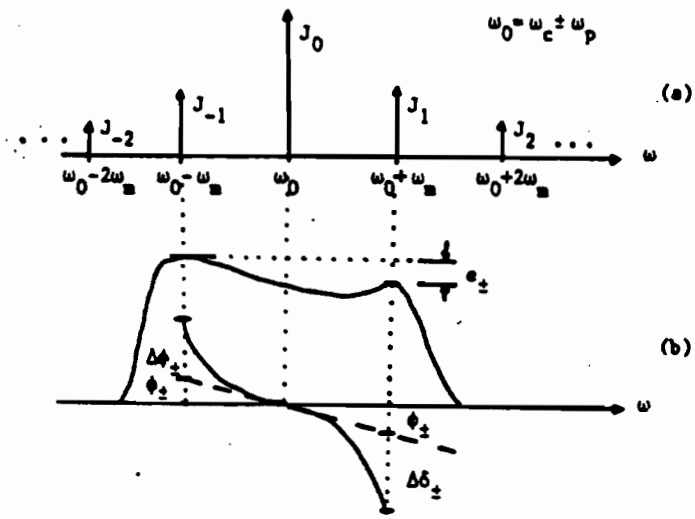

Fig. 8 (a) Spectrum of the SCPJ for $\phi(t) = \beta\cos(\omega_m t)$.
(b) Nonideal transfer function of the extraction filters $PBPF_\pm$, having bandwidth B' with $2f_m < B' < 4f_m$.

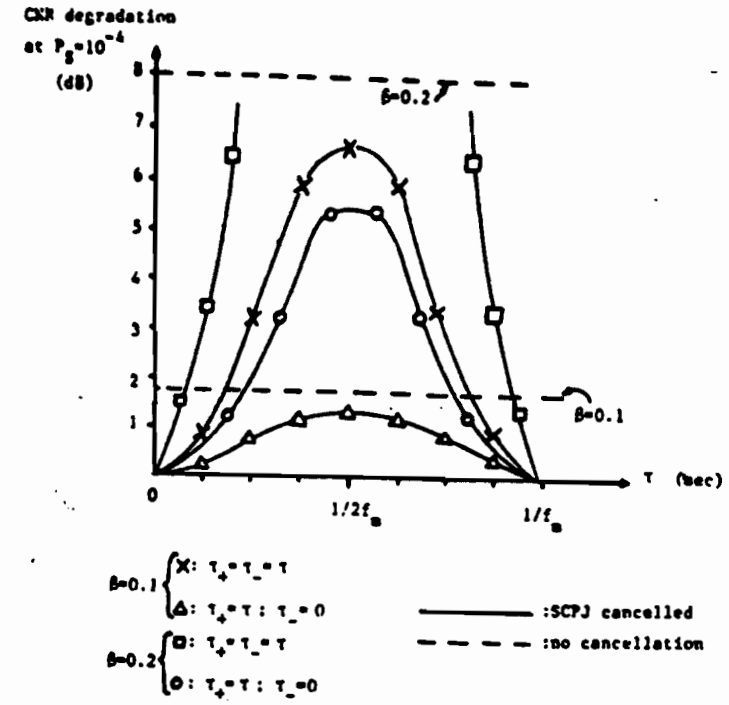

Fig. 7 CNR degradation of the DPS 16-QAM system for a wideband extraction filter and as a function of the constant group delay τ.

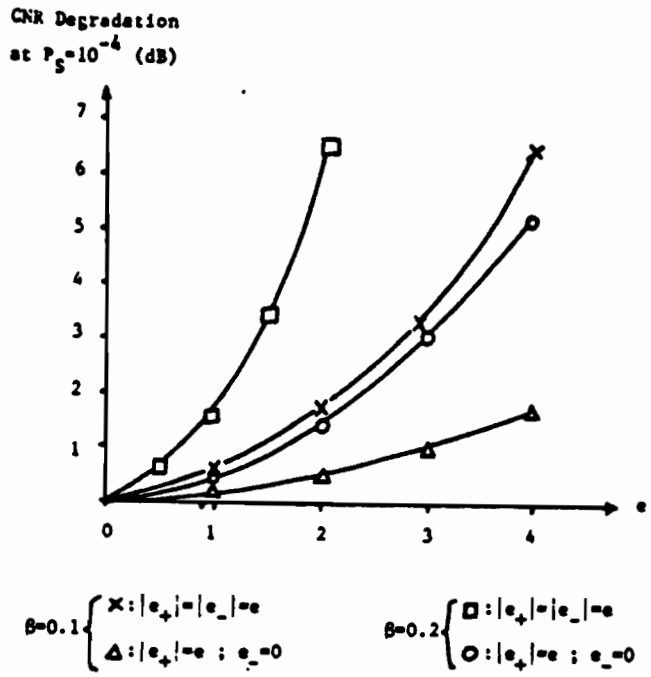

Fig. 9 CNR degradation of a 16-QAM DPS with narrowband extraction filters as a function of the amplitude variations e of the extraction filters, e.

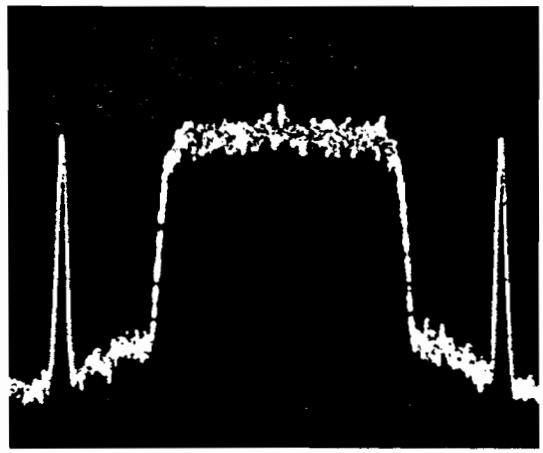

Fig. 12 Measured spectrum of the transmitted 16-QAM DPS without any Gaussian noise or System Caused Phase Jitter (SCPJ). The power, which is allocated to each of the pilot tones is 17 dB below the data signal power.
Horizontal Axis: 50 kHz/div
Vertical Axis: 10 dB/div
Center Frequency: 1.5 MHz
Resolution Bandwidth: 5 kHz.

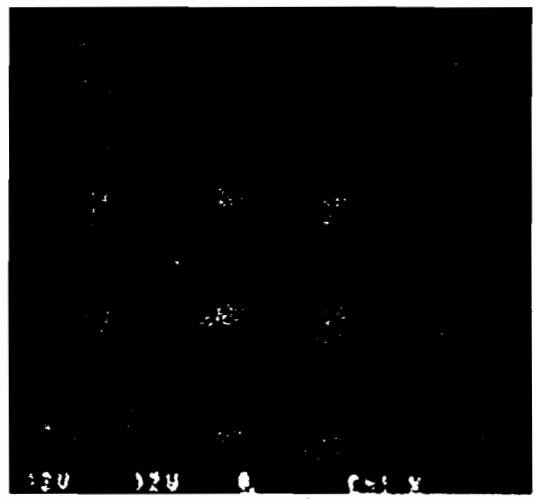

Fig. 13 Measured signal state space diagram of the demodulated 16-QAM DPS in the presence of sinusoidal (SCPJ) with β=0.1 & f_m=9 kHz and additive white Gaussian noise (C/N=22dB). Notice that the outer states are more smeared than the inner states.

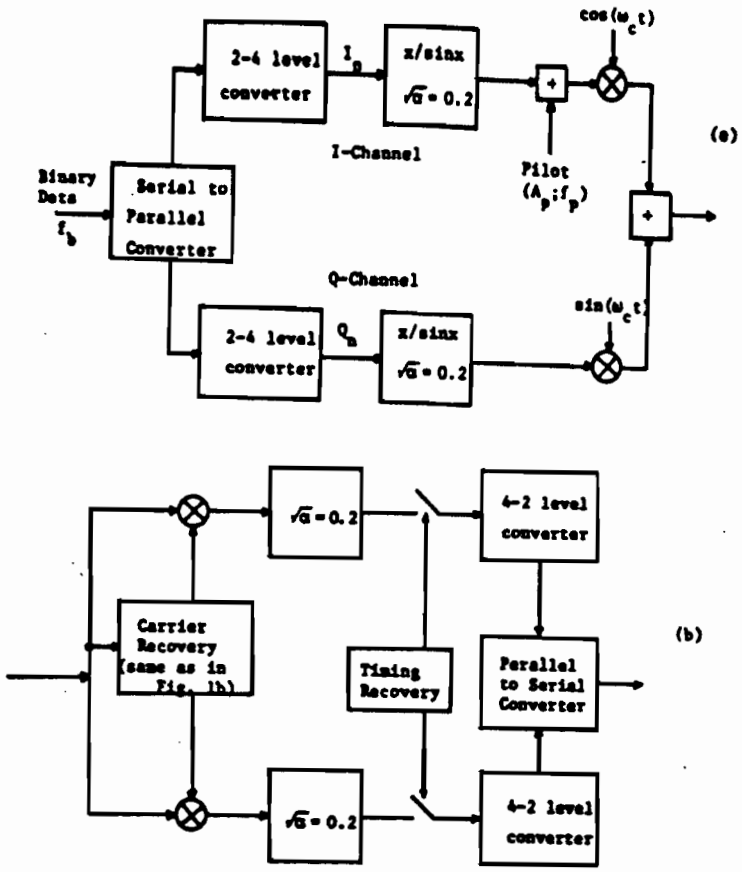

Fig. 11 Block diagram of the used experimental 16-QAM DPS.
(a) Transmitter.
(b) Receiver.

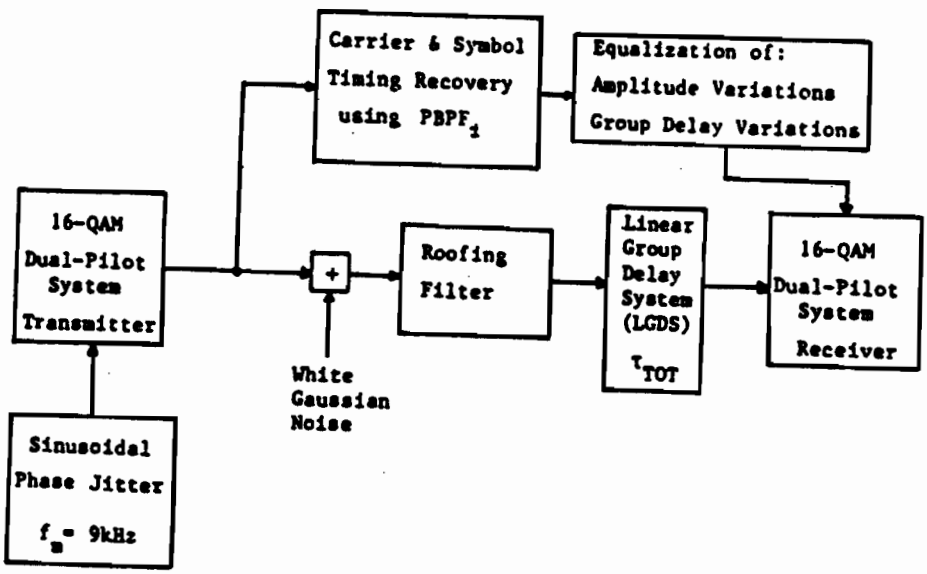

Fig. 14 Block diagram of the experimental setup used to test the 16-QAM DPS.

(130)

	Center Frequency f_0 (MHz)	Extraction Bandwidth B' (kHz)	Amplitude Variation ε	Group Delay at f_0 τ' (μsec)	Group Delay Variation Δτ' (μsec)
Filter Set 1 (S_1)	1.3	21	1.74	35	2
	1.7	22	1.78	35	1
Filter Set 2 (S_2)	1.3	61	1.95	30	20
	1.7	60	2.19	28	12

TABLE I

MEASURED CHARACTERISTICS OF THE USED EXTRACTION FILTER SETS

		Carrier-to-Noise (C/N) Degradation in dB at $P_e=10^{-4}$			
		Analytical Results		Measured Performance †	
		β=0.1	β=0.2	β=0.1	β=0.2
No phase jitter cancellation (B'=0)		1.8	8.0	2.0±0.2	Error floor at 10^{-3}
Partial phase jitter cancellation (Filter set S_1; B'=2.3f_m)	Partial distortion compensation ε'_r=0.3, τ'_r=10μs, $\Delta\tau'_r$=1μs	1.7	2.8	2.0±0.2	4.0±0.4
	Maximal group delay and amplitude compensation	0.2	0.5	0.5±0.2	0.9±0.2
Practically total phase jitter cancellation (Filter set S_2; B'=6.6f_m)	Partial distortion compensation ε'_r=0.1, τ'_r=10μs, $\Delta\tau'_r$=1μs	0.8	2.5	1.2±0.2	3.5±0.4
	Maximal group delay and amplitude compensation	≈0	≈0	≈0	0.2±0.1

† In order to have a direct comparison with the analytically derived results, these measured results do not include the 16-QAM modem back-to-back performance degradation, which was approximately 1.0dB. Furthermore, for the same reason, the additional carrier of 0.4dB, which is required to transmit the pilot tones is not included.

TABLE II

COMPARISON BETWEEN THE ANALYTICAL RESULTS AND THE MEASURED PERFORMANCE OF A 16-QAM DUAL PILOT SYSTEM OPERATED IN THE PRESENCE OF AMCH AND SINUSOIDAL SYSTEM CAUSED PHASE JITTER

II) Pilot Sequences

- Same idea as with pilot tones

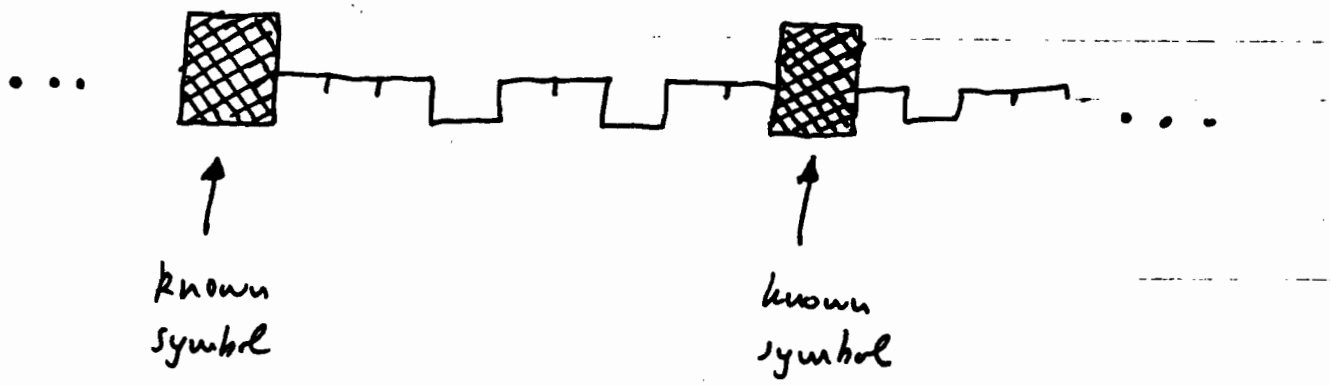

- Receiver : i/ extract the known symbol
  ii) "Undo" interference.

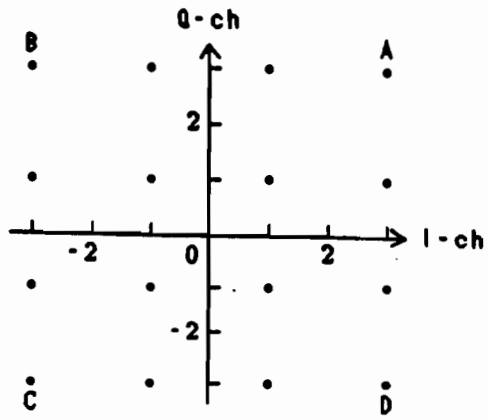

Fig.1 Signal state diagram of 16QAM.

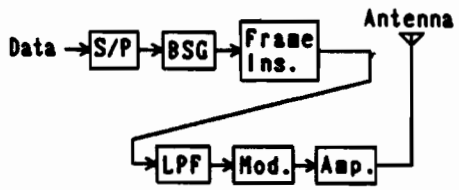

Fig.2 Configuration of the transmitter.

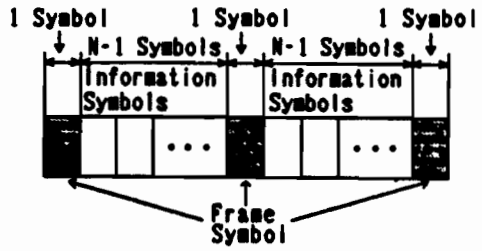

Fig.3 Frame format.

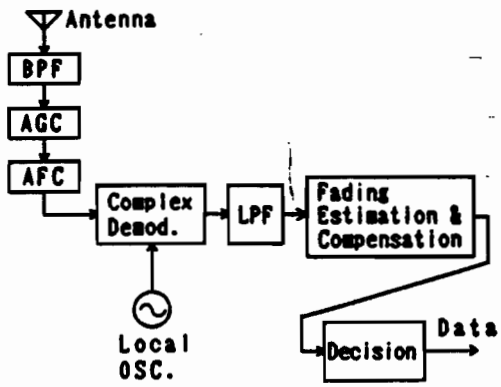

Fig.4 Configuration of the receiver.

Ref. Sampei & Sunaga
"Rayleigh fading compensation method for 16-QAM in digital mobile radio channels"
Proceedings of VTC 89.

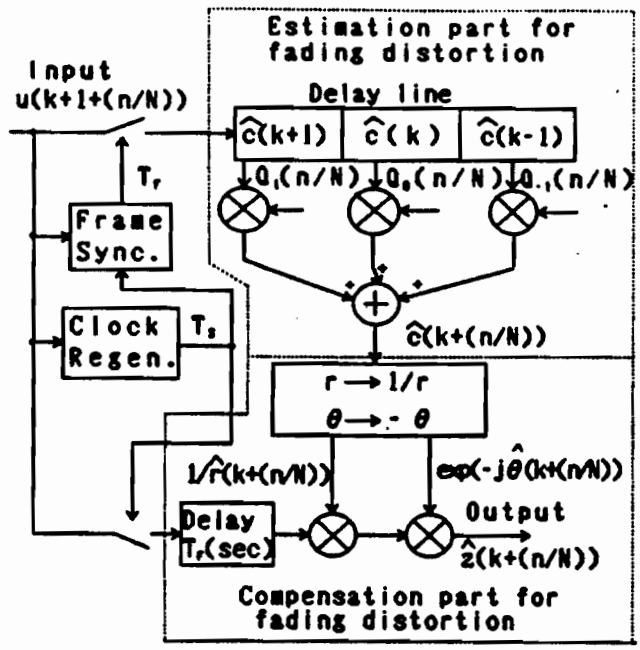

Fig.5 Configuration of the fading estimation and compensation part.

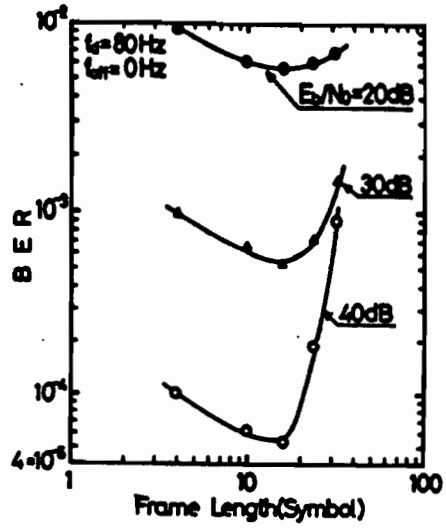

Fig.7 BER performance vs. N with the parameter E_b/N_0, where f_d=80Hz and f_{off}=0Hz.

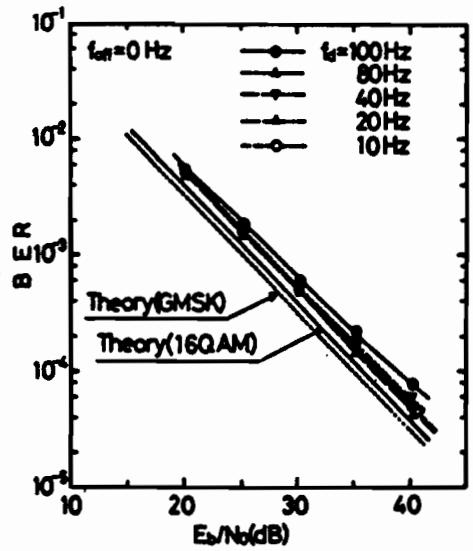

Fig.8 BER performance under Rayleigh fading environment (computer simulation).

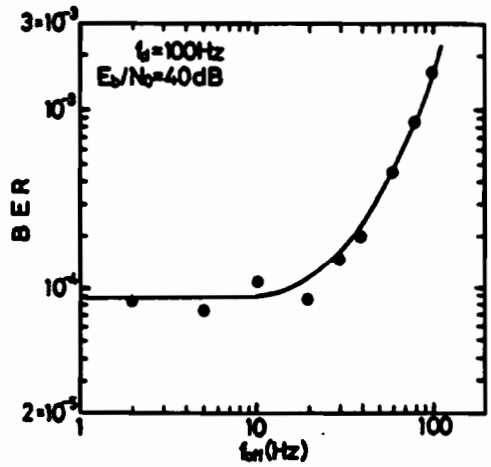

Fig.9 BER performance vs. f_{off}, where N=16, f_d=100Hz, and E_b/N_0=40dB.

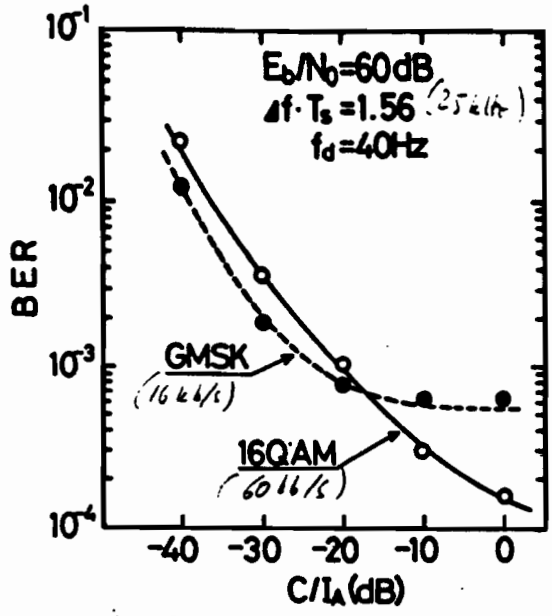

Fig.10 BER performance vs. C/I_A.

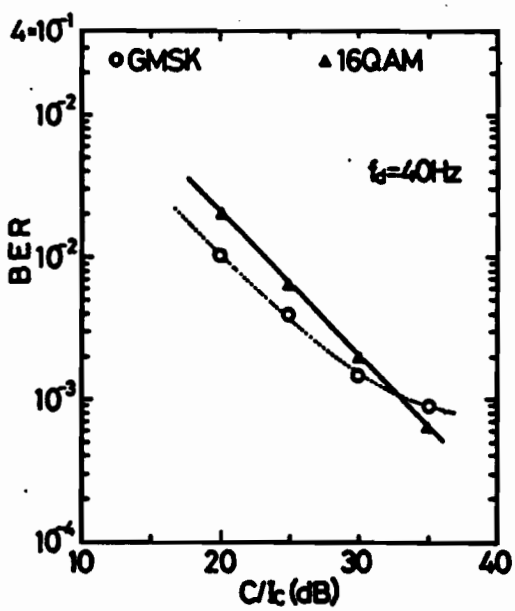

Fig.11 BER performance vs. C/I_C.

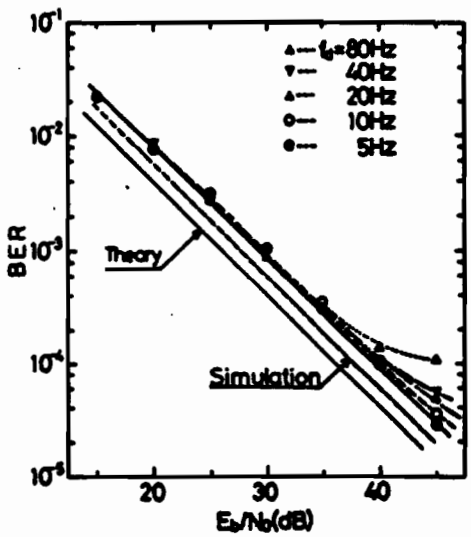

Fig.12 BER performance under Rayleigh fading environment(laboratory experiment).

DIFFERENTIALLY COHERENT SYSTEMS

(differential detection).

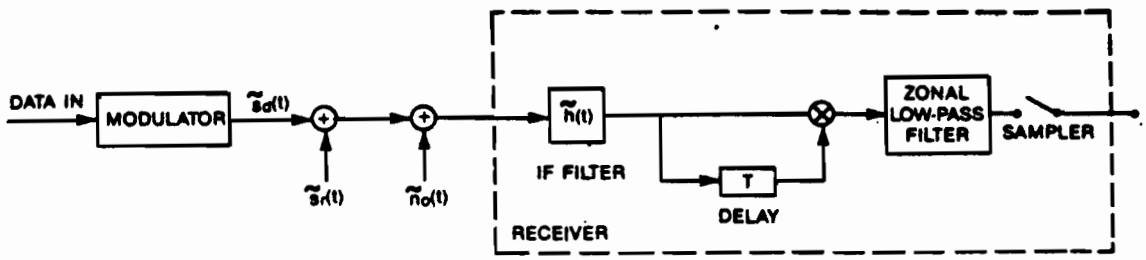

Fig. 1. Model of system.

TABLE I
SPECTRA AND AUTOCORRELATION FUNCTION OF FADING PROCESS $\xi(t)$

Denotation	Spectrum $S_\xi(f)$	Autocorrelation Function $R_\xi(\tau)$
1. Rectangular	$D/(2B_D)$ $\lvert f\rvert < B_D$ 0 elsewhere	$D \sin(2\pi B_D\tau)/(2\pi B_D\tau)$
2. Gaussian	$D \exp[-f^2/B_D^2]/\sqrt{\pi}\,B_D)$	$D \exp[-(\pi B_D\tau)^2]$
3. Land Mobile	$D/[\pi(f^2-B_D^2)^{1/2}]$	$D\,J_0(2\pi B_D\tau)$
4. First-order Butterworth	$D/[\pi B_D(1+f^2/B_D^2)]$	$D \exp[-2\pi B_D\lvert\tau\rvert]$
5. Second-order Butterworth	$D/(1+16f^4/B_D^4)$	$D \exp(-\beta\lvert\tau\rvert)\times$ $[\cos(\beta\tau)+\sin(\beta\lvert\tau\rvert)]$

Notes: 1. $J_0(\cdot)$ is the zero-order Bessel function of the first kind.
2. $\beta = \pi B_D/\sqrt{2}$ in the second-order Butterworth spectrum.

Ref: Mason, "Error probability evaluation for systems employing differential detection in a fast Ricean fading environment."

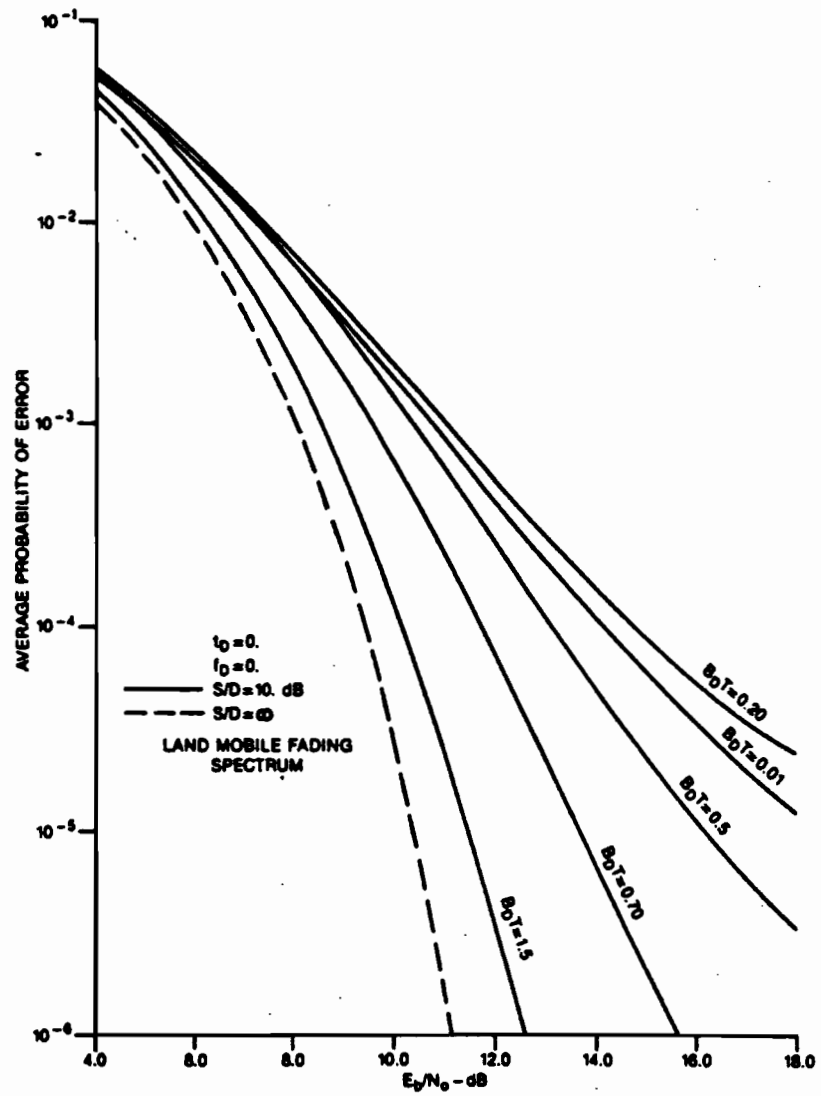

Fig. 2. Probability of error for differential detection of BPSK with a matched filter for different fading bandwidths $B_D T$.

TABLE III
EXAMPLE OF FADING COMPONENT COVARIANCES FOR A RECTANGULAR FADING SPECTRUM, AND $B_D T = 0.1$

$\Delta\tau/T$	$r_{\downarrow 1}/D$	$r_{\downarrow 2}/D$
1/8	0.992	0.946 + j 0.199
1/16	0.990	0.945 + j 0.203
1/32	0.990	0.945 + j 0.203
1/64	0.990	0.945 + j 0.203

TABLE IV
REQUIRED E_b/N_0 FOR $P(e) = 10^{-2}$ FOR DIFFERENTIAL DETECTION OF MSK USING FOURTH-ORDER BUTTERWORTH FILTER WITH $BT = 1.2$. $S/D = 9$ dB.

Fading Bandwidth ($B_D T$)	Spectrum				
	Rectangular	Gaussian	Land Mobile	First order Butterworth	Second order Butterworth
0.01	9.1	9.1	9.1	9.1	9.1
0.10	9.1	9.2	9.2	9.3	9.1
0.30	9.7	9.7	10.0	9.2	9.4
0.50	10.2	9.9	10.4	8.9	9.7
0.70	10.1	9.7	9.8	8.6	9.8
1.00	9.4	9.2	8.9	8.4	9.7

fading component bandwidth and spectral shape on error probability for this example is examined.

TABLE II
NORMALIZED COVARIANCES FOR LAND MOBILE FADING

Fading Bandwidth (B_DT)	$r_{\downarrow\downarrow}(T)/D$	$r_{\downarrow 2}(T)/D$
0.01	1.000	0.999
0.20	0.937	0.613
0.50	0.677	-0.058
0.70	0.490	-0.035
1.50	0.216	-0.005

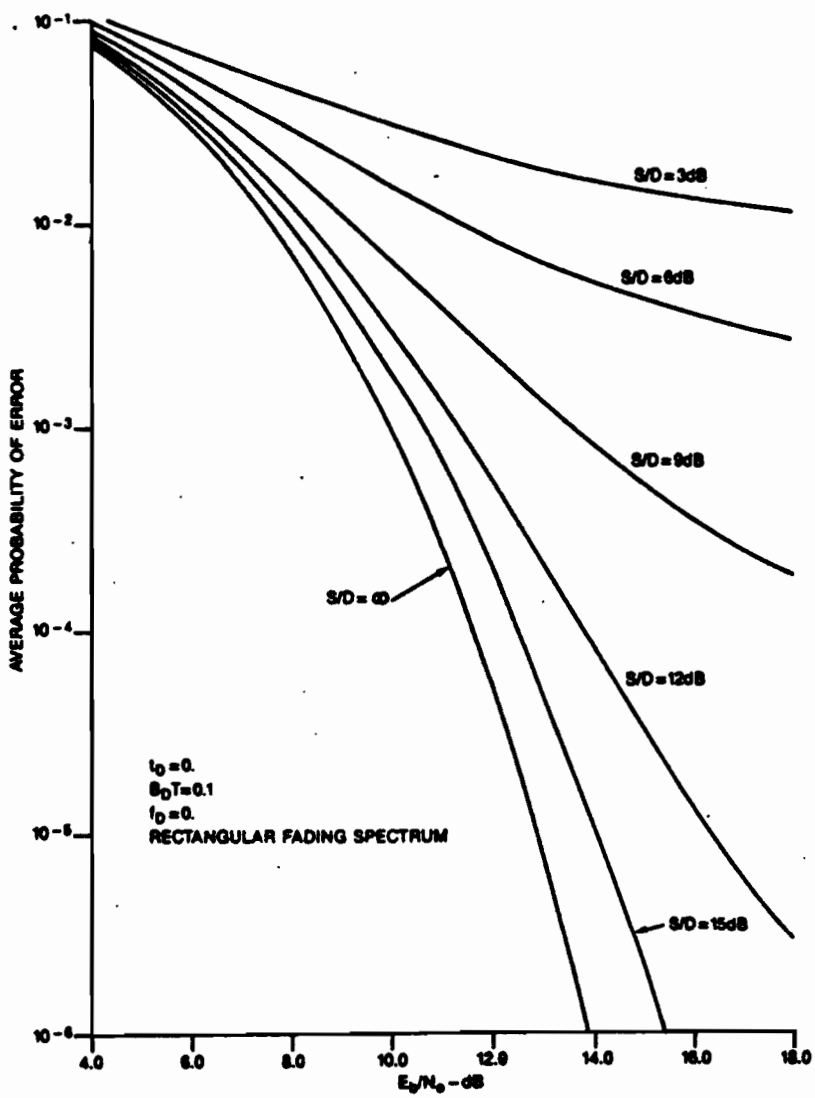

Fig. 4. Probability of error for the differential detection of MSK. A fourth-order Butterworth filter with $BT = 1.20$ was used.

$\frac{\pi}{4}$-QPSK - dd

32K symbols, sps=16, alpha=0.35

R=2.4 KBps, no time dispersion

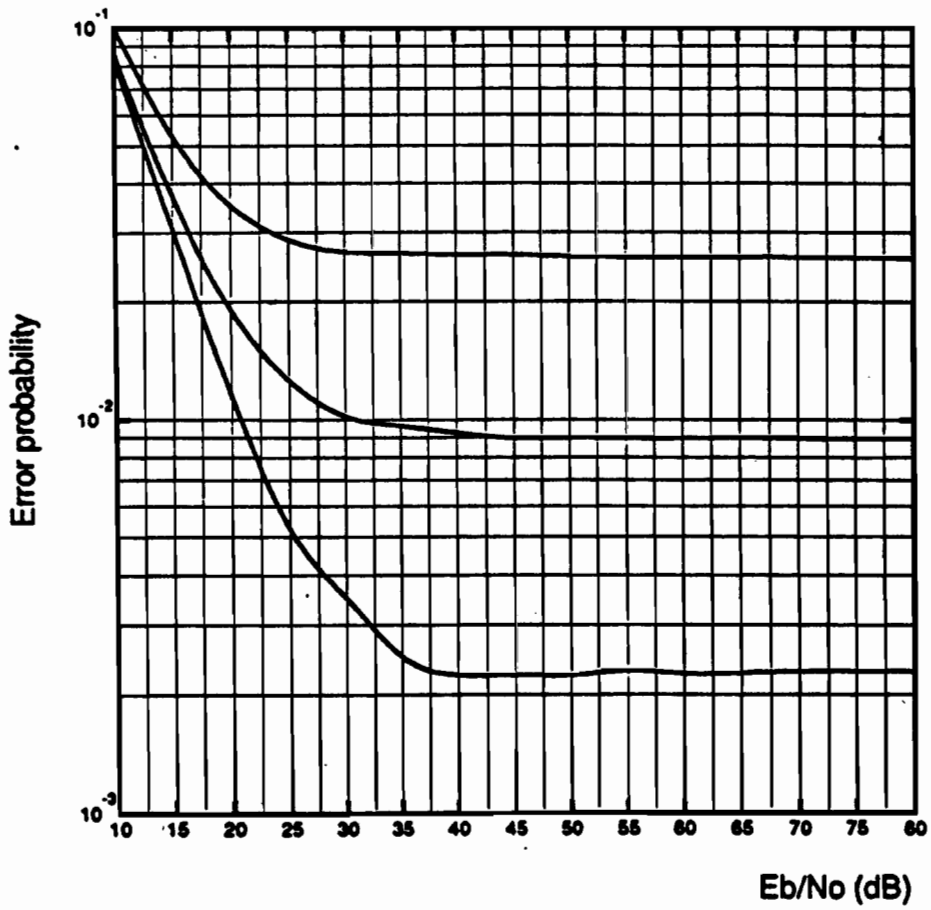

π/4 - QPSK - dd

64K symbols, sps=16, alpha=0.2

R=2.4 KBps, no time dispersion

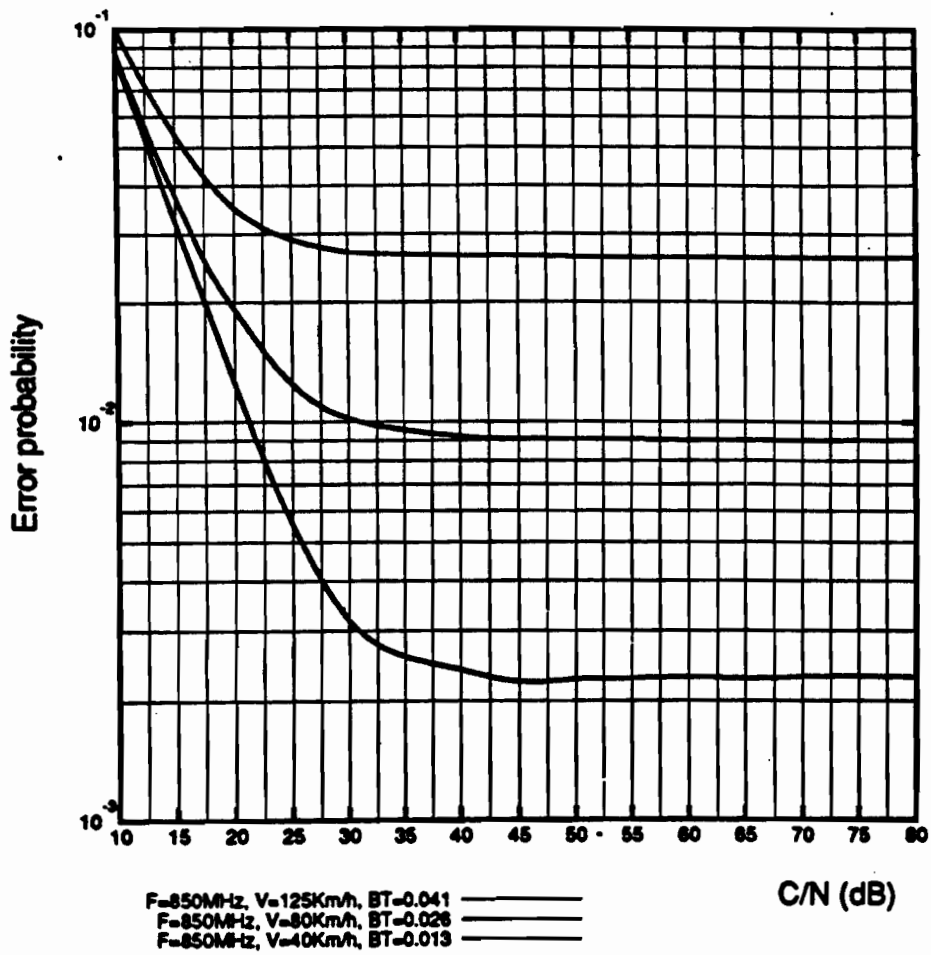

π/4 - QPSK - dd

128K symbols, 64K window, sps=16, alpha=0.2

R=24 KBps, no time dispersion

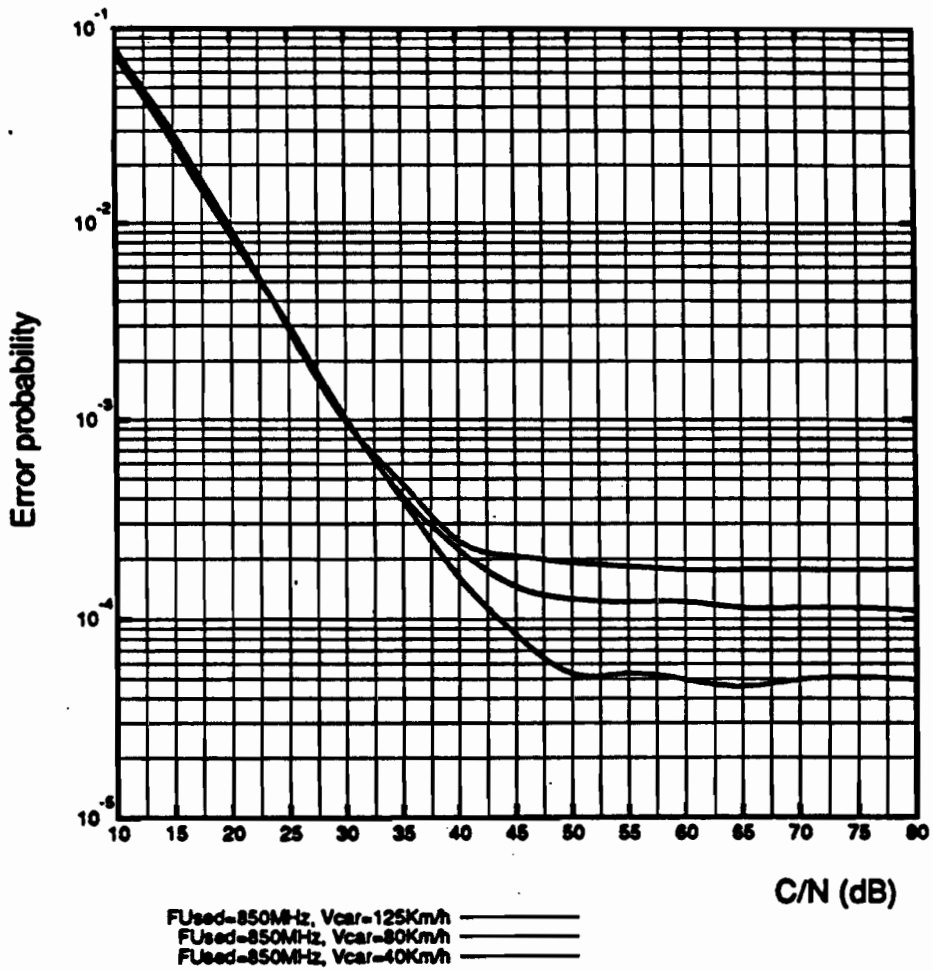

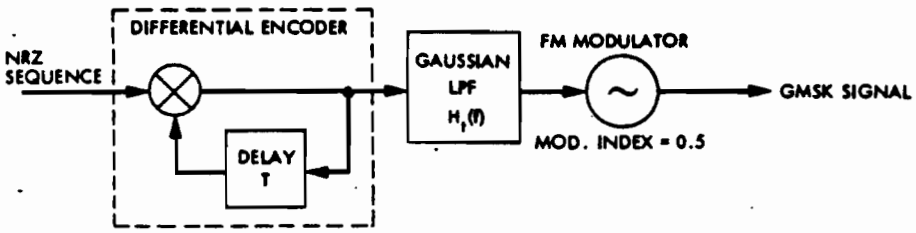

Fig. 1. A GMSK transmitter.

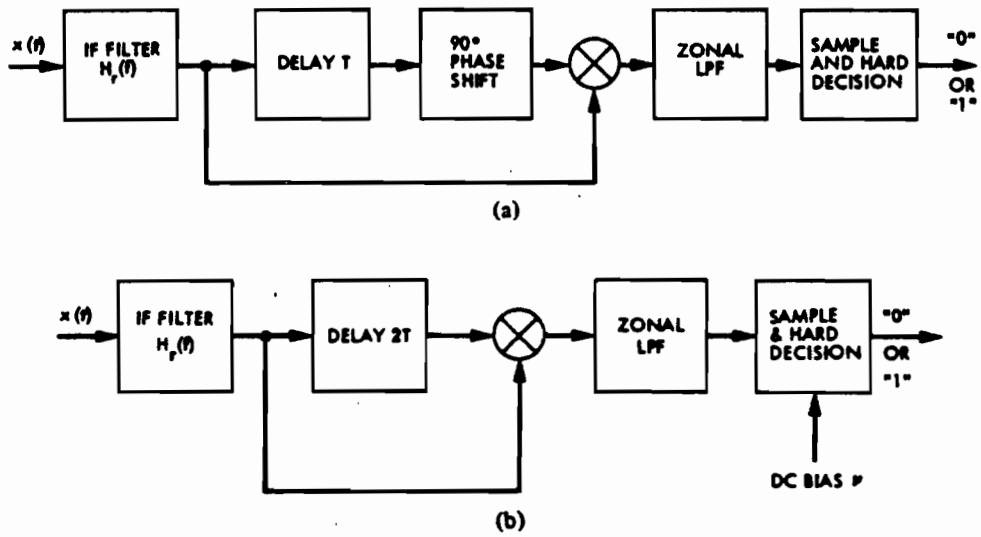

Fig. 2. (a) A one-bit differential detector for GMSK. (b) A two-bit differential detector for GMSK.

Ref. Simon & Wang, "Differential detection of GMSK in a mobile radio environment," IEEE Trans. Veh. Techn., Nov. 84.

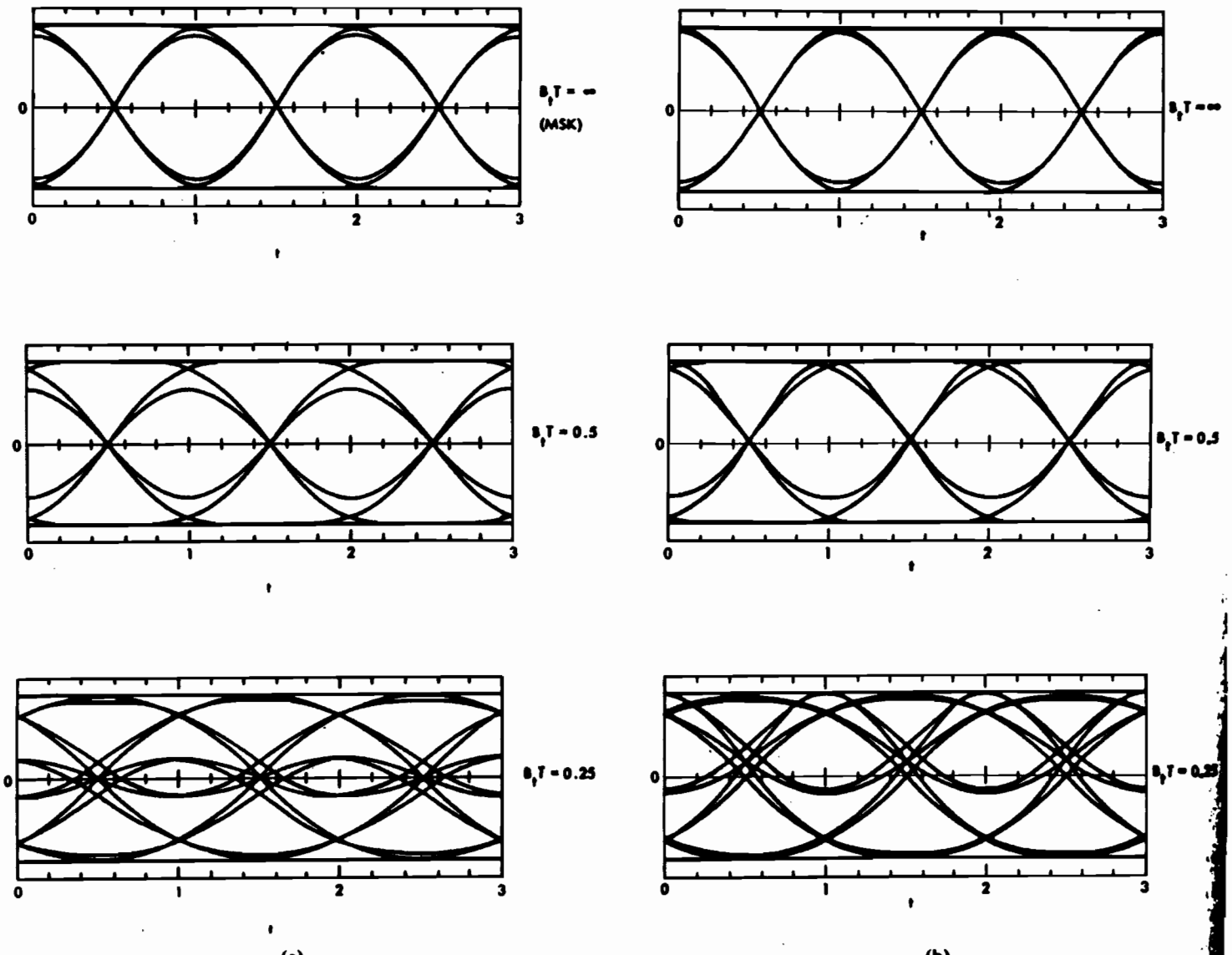

Fig. 3. (a) One-bit detector eye patterns; Gaussian IF receiver filter; $B_IT = 1.25$. (b) Two-bit detector eye patterns; Gaussian IF receiver filter; $B_IT = 1.25$.

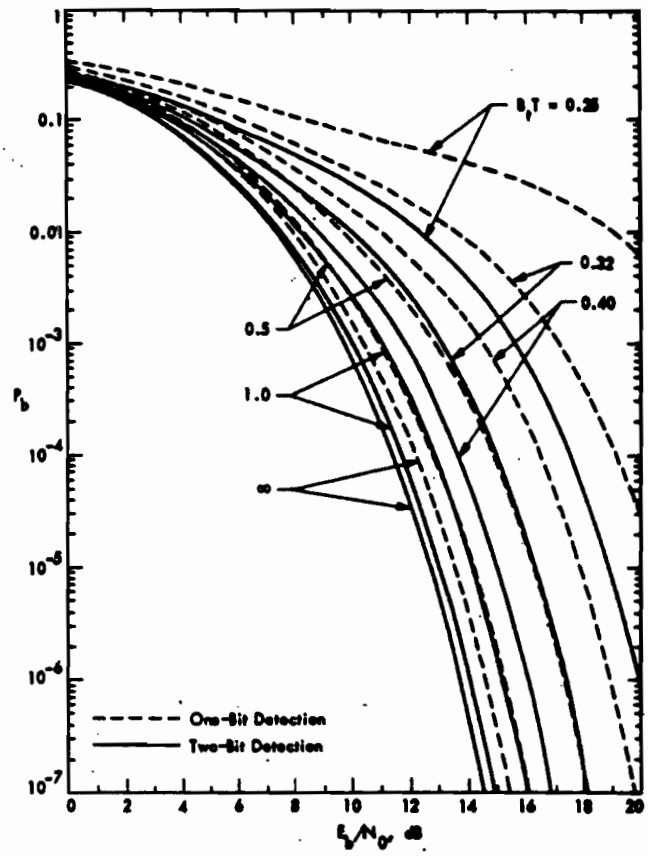

Fig. 7. Performance of one- and two-bit differential detection of GMSK; receiving B_iT is optimized for each B_iT. (For two-bit detection case, detection threshold is optimized for each E_b/N_0.)